Chemistry–A European Journal
Research Article
doi.org/10.1002/chem.202301371
Chemistry Europe
European Chemical Societies Publishing
www.chemeurj.org

Hot Paper

The Oxidation of Oxygen and Sulfur-Containing Heterocycles by Cytochrome P450 Enzymes

Matthew N. Podgorski,[a] Angus B. Keto,[b] Tom Coleman,[a] John B. Bruning,[c] James J. De Voss,[b] Elizabeth H. Krenske,*[b] and Stephen G. Bell*[a]

The cytochrome P450 (CYP) superfamily of monooxygenase enzymes play important roles in the metabolism of molecules which contain heterocyclic, aromatic functional groups. Here we study how oxygen- and sulfur-containing heterocyclic groups interact with and are oxidized using the bacterial enzyme CYP199A4. This enzyme oxidized both 4-(thiophen-2-yl)benzoic acid and 4-(thiophen-3-yl)benzoic acid almost exclusively via sulfoxidation. The thiophene oxides produced were activated towards Diels-Alder dimerization after sulfoxidation, forming dimeric metabolites. Despite X-ray crystal structures demonstrating that the aromatic carbon atoms of the thiophene ring were located closer to the heme than the sulfur, sulfoxidation was still favoured with 4-(thiophen-3-yl)benzoic acid. These results highlight a preference of this cytochrome P450 enzyme for sulfoxidation over aromatic hydroxylation. Calculations predict a strong preference for homodimerization of the enantiomers of the thiophene oxides and the formation of a single major product, in broad agreement with the experimental data. 4-(Furan-2-yl)benzoic acid was oxidized to 4-(4′-hydroxybutanoyl)benzoic acid using a whole-cell system. This reaction proceeded via a γ-keto-α,β-unsaturated aldehyde species which could be trapped in vitro using semicarbazide to generate a pyridazine species. The combination of the enzyme structures, the biochemical data and theoretical calculations provides detailed insight into the formation of the metabolites formed from these heterocyclic compounds.

Introduction

Heterocyclic and aromatic moieties are commonly found in drug molecules.[1] As of 2014, drugs containing nitrogen and sulfur heterocycles comprise >60% of all FDA-approved compounds,[2] and benzene rings are the most common ring system found in these pharmaceuticals.[3] Heterocyclic furan rings are also found in chemicals across food and herbal and synthetic medicines and are often toxic.[4] The metabolism of these heterocyclic, aromatic functional groups by cytochrome P450 enzymes (CYP) is thus of great significance for researchers in the pharmaceutical industry. P450 enzymes are capable of catalyzing the oxidation of aromatic systems, usually with hydroxylation as the outcome. However, the bond dissociation energy of an aromatic C–H bond is significantly higher than that of an alkyl C-H bond.[5] Thus, in these reactions, rather than direct abstraction of the C–H hydrogen, it is the aromatic π-electron system which reacts with the reactive intermediate of the P450 enzymes, the species designated compound I (Cpd I; a ferryl-oxo porphyrin cation radical; Scheme 1).[6] As a result, the reactions of aromatic substrates are mechanistically different to aliphatic C–H bond hydroxylations.[7]

One of the mechanisms proposed for aromatic oxidations involves formation of an epoxide intermediate, followed by migration of a hydrogen to form a ketone. Subsequent enolization regenerates the aromaticity of the product. This mechanism was invoked to explain the observation of the "NIH shift" in which a hydrogen isotope at the site of oxidation is observed in the product at an adjacent carbon (Scheme 1).[8] Subsequent studies have directly observed and characterized epoxides and oxepins in certain aromatic oxidations,[9] but others propose there are cases where a Fe(IV)–O–C intermediate would preferably be generated (Scheme 1).[7b,10] This reaction mechanism is also referred to as *ipso*-substitution and arises from electrophilic attack of Cpd I on the aromatic ring; hydrogen migration and rearomatization would give the product and explain the NIH shift. It has also been hypothesized that these two mechanistic proposals, oxepin formation and *ipso*-substitution, can have other steps which contribute to the overall rate including electron transfer processes.[7a,11]

As heterocycles feature prominently in drug molecules their metabolism by cytochrome P450 enzymes has been investigated.[1,2b,12] Nitrogen-containing pyridinyl, imidazolyl and triazolyl compounds can interact with the heme via the nitrogen and inhibit cytochrome P450 enzymes.[13] Therefore, a

[a] M. N. Podgorski, Dr. T. Coleman, Dr. S. G. Bell
Department of Chemistry
University of Adelaide
Adelaide, SA, 5005 (Australia)
E-mail: stephen.bell@adelaide.edu.au
[b] A. B. Keto, Prof. J. J. De Voss, Dr. E. H. Krenske
School of Chemistry and Molecular Biosciences
University of Queensland
Brisbane, Qld, 4072 (Australia)
E-mail: e.krenske@uq.edu.au
[c] Dr. J. B. Bruning
School of Biological Sciences
University of Adelaide
Adelaide, SA 5005 (Australia)

Supporting information for this article is available on the WWW under https://doi.org/10.1002/chem.202301371

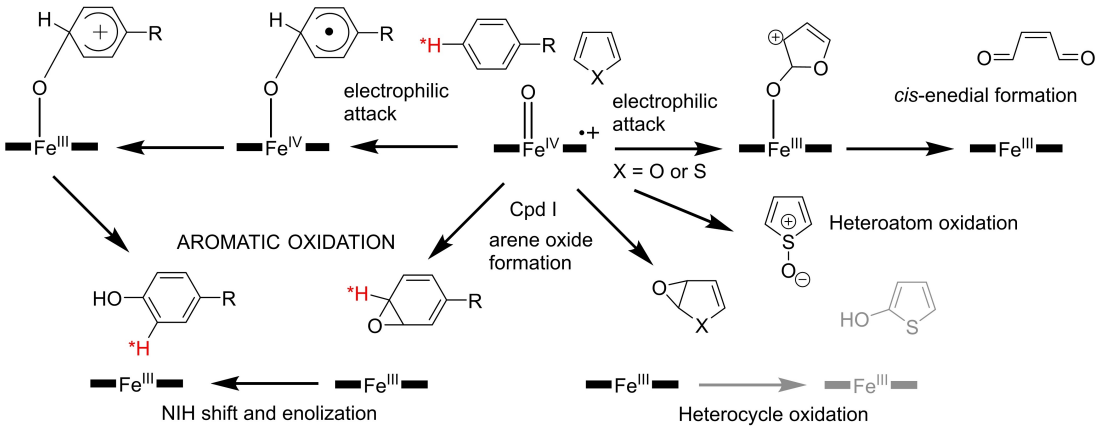

Scheme 1. The product formation pathways involved in aromatic hydroxylation by a P450 enzyme. In aromatic hydroxylation the reaction can proceed via formation of an arene oxide (NIH mechanism, H* denotes the shift of the hydrogen atom or a deuterium) or electrophilic attack of Cpd I on the aromatic π system. The oxygen or sulfur heteroatom in five-membered aromatic systems in furan and thiophene rings can result in different types of reactivity being observed.

detailed understanding of how they interact with the heme and their metabolic pathways is critical in effective drug design.[14] Furan-containing compounds can also function as inhibitors of P450 enzymes, but under certain conditions may be metabolized.[4,15] For example, the furanocoumarin family of compounds can undergo oxidation to furan epoxides, which cause mechanism-based inhibition of microsomal CYP2A6 and CYP2B1.[15a,b,16] More recent studies have shown that the ring-opening metabolism of a simple furan molecule by human and rat liver P450s yields a highly liver-toxic α,β-unsaturated dialdehyde (*cis*-enedial or γ-ketoenal).[17] Thiophenes have also been shown to undergo oxidation via a number of pathways with P450 enzymes.[18] With certain thiophene substrates, inhibition of microsomal P450 enzymes has been observed.[19] However, there are examples of P450-catalyzed sulfoxidation of thiophenes, resulting in an unstable intermediate which can undergo subsequent reactions including a Diels–Alder dimerization.[18a,e,20] Additionally, cytochrome P450 enzymes have been reported to catalyze thiophene aromatic C–H hydroxylations and the epoxidation of thiophenes.[18b–d]

We have used the bacterial CYP199A4 enzyme as a model system to study different cytochrome P450 activities.[21] This enzyme from *Rhodopseudomonas palustris* strain HaA2 catalyzes the oxidation of *para*-substituted benzoic acids, including aromatic oxidations and sulfoxidations.[14b,22] For example, it can efficiently oxidatively demethylate 4-methoxybenzoic acid. It is a useful system as it can work with a range of substituted benzoic acids and an efficient electron transfer system has been identified. The electron transfer system consists of a flavin dependent reductase (HaPuR) and a 2Fe-2S ferredoxin (HaPux).[22a] In addition, the CYP199A4 system has been structurally characterized.[21b,c,22b,c] As a result, this enzyme has been used to investigate the different parameters required for aliphatic and aromatic oxidation by using 4-cyclohexylbenzoic acid and 4-phenylbenzoic acid. While both substrates bound within the enzyme active site in a similar manner, aliphatic oxidation of 4-cyclohexylbenzoic acid was catalyzed but aromatic oxidation of 4-phenylbenzoic acid was not.[7c]

Furan and thiophene rings are more reactive than phenyl rings. We have demonstrated that CYP199A4 can catalyze the oxidation of imidazole rings, while triazoles act as inhibitors.[14a,23] In order to study how oxygen and sulfur heterocyclic functional groups interact with and are oxidized by P450 enzymes, *para*-substituted furan and thiophene benzoic acids were investigated with CYP199A4 (Figure 1). 4-(Furan-2-yl)benzoic acid, 4-(thiophen-2-yl)benzoic acid and 4-(thiophen-3-yl)benzoic acid were screened with CYP199A4 to investigate the binding of these compounds, and to identify oxidation products (Figure 1).

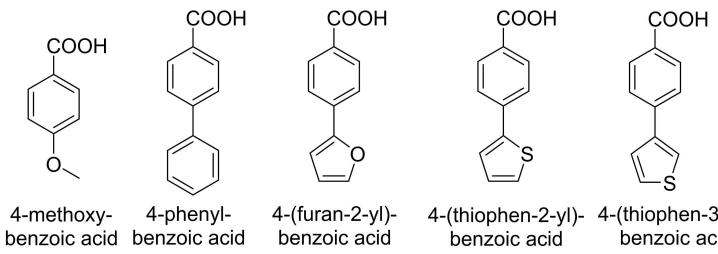

Figure 1. The CYP199A4 substrates investigated in or relevant to this study.

Results and Discussion

Substrate binding

Substrate binding to CYP199A4 was monitored by UV-vis spectroscopy. The addition of 4-(thiophen-3-yl)benzoic acid to CYP199A4 resulted in a 90% shift from the low-spin (Soret band at ~418 nm) to the high-spin form of the ferric heme (Soret band at ~395 nm; Figure 2). The binding affinity was measured by using UV-vis titrations to determine the dissociation constant, K_d, 0.51 ± 0.07 μM, which is comparable to the value obtained previously for 4-phenylbenzoic acid (K_d 0.65 ± 0.07 μM, Table 1, Figure S1).[7c] A similar switch to the high-spin state (75%, Figure 2) and binding affinity were observed with 4-(thiophen-2-yl)benzoic acid (K_d 0.60 ± 0.10 μM, Table 1, Figure S1). Addition of 4-(furan-2-yl)benzoic acid to CYP199A4 induced a lower 35% shift to the high-spin ferric state (Figure 2 and Table 1). The dissociation constant was measured as 2.7 ± 0.3 μM indicating a lower binding affinity than the thiophenes (Figure S1).

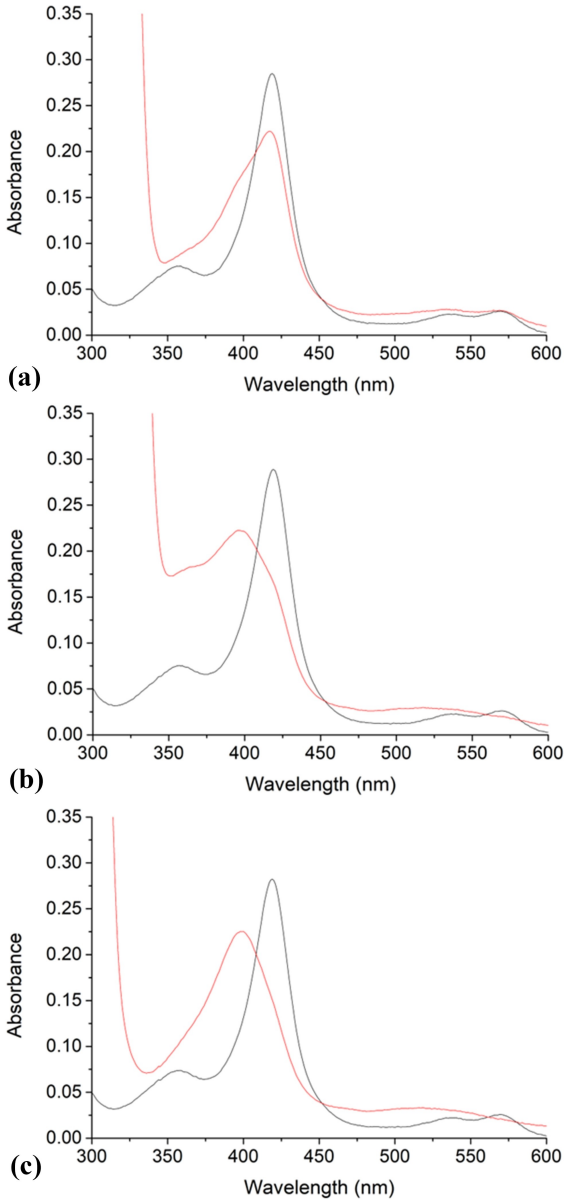

Figure 2. UV-vis analysis of the spin state of CYP199A4 with selected aromatic *para*-substituted furanyl and thiophenyl benzoic acids. a) 4-(furan-2-yl)benzoic acid, b) 4-(thiophen-2-yl)benzoic acid and c) 4-(thiophen-3-yl)benzoic acid. The substrate-free form is shown in black and the substrate-bound form in red.

Table 1. Substrate binding and in vitro turnover data for CYP199A4 and selected substrates.

Substrate (BA benzoic acid)	HS [%][a]	K_d [μM][b]	NADH[c] [min^{-1}]
4-(furan-2-yl)BA	35%	2.7 ± 0.3	200 ± 6
4-(thiophen-2-yl)BA	75%	0.60 ± 0.10	118 ± 3
4-(thiophen-3-yl)BA	90%	0.51 ± 0.07	19 ± 1
4-phenylBA[d,7c]	90%	0.65 ± 0.07	902 ± 34
4-methoxyBA[14b]	≥95%	0.28 ± 0.01	1340 ± 30

[a] HS is the percentage of high-spin ferric heme of CYP199A4 after the addition of substrate as measured by UV-vis spectroscopy. [b] K_d the dissociation constant as measured by UV-vis titrations. [c] NADH is the rate of NADH oxidation, including product formation and uncoupling reactions. The NADH consumption ("leak rate") of the system in the absence of a substrate was measured to be ~9.0 min^{-1}. The turnovers were measured using a HaPuR:HaPux:CYP199A4 concentration ratio of 1:10:1 (0.5 μM CYP enzyme, 50 mM Tris, pH 7.4). Rates are reported as mean ± S.D. ($n \geq 3$) and given in nmol nmol-CYP^{-1} min^{-1} (abbreviated to min^{-1}). [d] No detectable product formation was observed with 4-phenylbenzoic acid.

Substrate oxidation

In vitro oxidation reactions with CYP199A4, supported by the physiological HaPuR and HaPux electron transfer proteins, were undertaken. The rate of turnover of the catalytic cycle, as measured by the rate of NADH oxidation, did not follow the same trend as the proportion of high-spin heme content of CYP199A4 after substrate addition (Table 1). Oxidation of 4-(furan-2-yl)benzoic acid resulted in the highest NADH oxidation rate (200 ± 6 nmol nmol-CYP^{-1} min^{-1} henceforth abbreviated to min^{-1}) and 4-(thiophen-3-yl)benzoic acid the lowest (19 ± 1 min^{-1}; Table 1, Figure S2).

When these in vitro oxidation reactions were analyzed using GC-MS, no obvious P450 oxidation products were observed (Figure S3 and Figure S4). One metabolite peak (*m/z* 364.20) was identifiable from the oxidation of 4-(thiophen-2-yl)benzoic acid in the GC-MS chromatogram (the mass was equivalent to that of the derivatized substrate (276) plus 88 as would be expected for a hydroxylation metabolite after addition of a trimethylsilyl group from derivatization). However, the levels of this metabolite were very low and the position of hydroxylation has not been established (Figure S3 and Figure S4).

HPLC analysis was more informative and revealed the formation of two significant metabolite peaks in a roughly 10:1 ratio after the oxidation of 4-(thiophen-2-yl)benzoic acid. A single major product could be identified in the 4-(thiophen-3-

yl)benzoic acid oxidation reaction (Figure 3). Control reactions confirmed that these metabolites arose from P450-catalyzed oxidation and not from a reaction with H_2O_2 (which can be generated via uncoupling during the P450 catalytic cycle; Figure S5). HPLC analysis of the CYP199A4-catalyzed oxidation of 4-(furan-2-yl)benzoic acid was less conclusive but a potential metabolite with an early retention time (4.6 min) was observed in the chromatogram (Figure 4). A control reaction confirmed that this metabolite did not arise from a reaction with H_2O_2.

Whole-cell oxidation to generate and identify the metabolites

In order to identify any potential metabolites we conducted whole-cell oxidation reactions using an *E. coli*-based system we have developed previously.[22a] HPLC analysis demonstrated that we were able to generate the same metabolites that were observed in the in vitro oxidation reactions with both thiophene substrates using the whole-cell oxidation system (Figure 3). The oxidation of 4-(thiophen-2-yl)benzoic acid generated significantly higher levels of product (Figure 3) and the whole-cell system was able to convert almost all of the 4 mM substrate that was added (~160 mg in 200 mL). The oxidation of 4-(furan-2-yl)benzoic acid in the whole-cell reactions formed a different metabolite to that observed in the in vitro oxidation reactions (Figure 4). Control experiments, including using *E. coli* cells transformed with a blank vector (no P450 production), were conducted to demonstrate that the metabolites observed in these reactions were only formed in the presence of the P450 enzyme (Figures 4 and S6).

GC-MS analysis of BSTFA/TMSCl-derivatized whole-cell reactions of the thiophene substrates were as inconclusive as those of the in vitro oxidations. No metabolite peaks were observed for 4-(thiophen-3-yl)benzoic acid. GC-MS analysis of the 4-

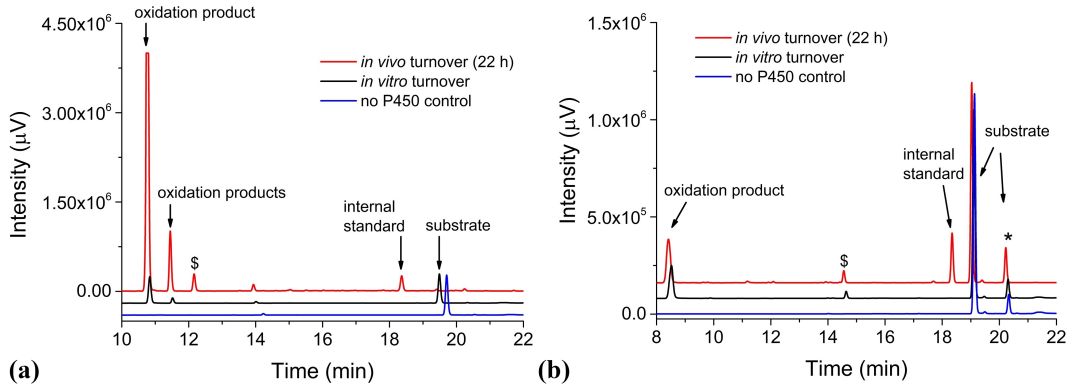

Figure 3. HPLC analysis of the in vivo (red) and in vitro NADH-driven (black) turnovers of a) 4-(thiophen-2-yl)benzoic acid and b) 4-(thiophen-3-yl)benzoic acid by CYP199A4. In blue is an in vitro control reaction omitting the P450. The in vivo (whole-cell) reaction mixture was analyzed after the reaction had been allowed to proceed for 22 h. The internal standard (where present; 9-hydroxyfluorene) appears at retention time (RT) 18.4 min. Note, there is an impurity in the 4-(thiophen-3-yl)benzoic acid substrate (RT 20.2 min; marked with an asterisk). A dollar sign ($) has been used to mark peaks which are potential oxidation metabolites, but have not yet been identified.

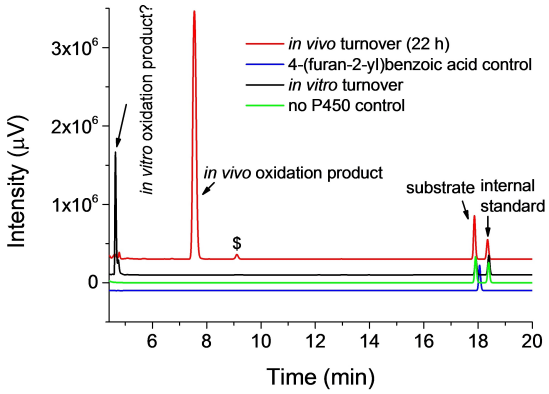

Figure 4. HPLC analysis of the in vivo (red) turnover and in vitro (black) NADH-driven turnover of 4-(furan-2-yl)benzoic acid by CYP199A4. In blue is the substrate control. In green is an in vitro "no P450" control reaction. The internal standard (9-hydroxyfluorene) appears at 18.4 min. In the in vitro reaction, there is a peak at 4.6 min which does not appear in the "no P450" control reaction. This peak may correspond to a P450 oxidation product. The in vivo (whole-cell) reaction mixture was analyzed after the reaction had been allowed to proceed for 22 h. A dollar sign ($) has been used to mark peaks which are potential reaction products, but have not yet been identified.

(furan-2-yl)-benzoic acid reaction did reveal two major metabolites (Figure S7). These had masses of +2 and +92 relative to the substrate indicating they did not arise from simple hydroxylation or epoxidation products (Figure S7).

The major metabolites from the whole-cell oxidation of all three substrates were purified by HPLC and analyzed by NMR in order to determine their identity. We were also able to obtain enough of the purified form of a minor metabolite from 4-(thiophen-2-yl)benzoic acid to enable NMR analysis. The major metabolite of 4-(furan-2-yl)benzoic acid oxidation was identified as 4-(4′-hydroxybutanoyl)benzoic acid by NMR and high-resolution mass spectrometry (Scheme 2, Figures S8 and S9). The mass of 4-(4′-hydroxybutanoyl)benzoic acid is 208.0736 Da. Ions were observed at *m/z* 209.0848 (corresponding to the protonated molecule), *m/z* 226.1015 (NH_4^+ adduct) and *m/z* 231.0634 (Na^+ adduct), consistent with the proposed metabolite (Figure S9). This is in agreement with the GC-MS analysis which showed a TMS-derivatized metabolite with a mass of 352 (+92 compared to the derivatized substrate; Figures S10 and S7). In addition, the metabolite observed with a mass of 262 (+

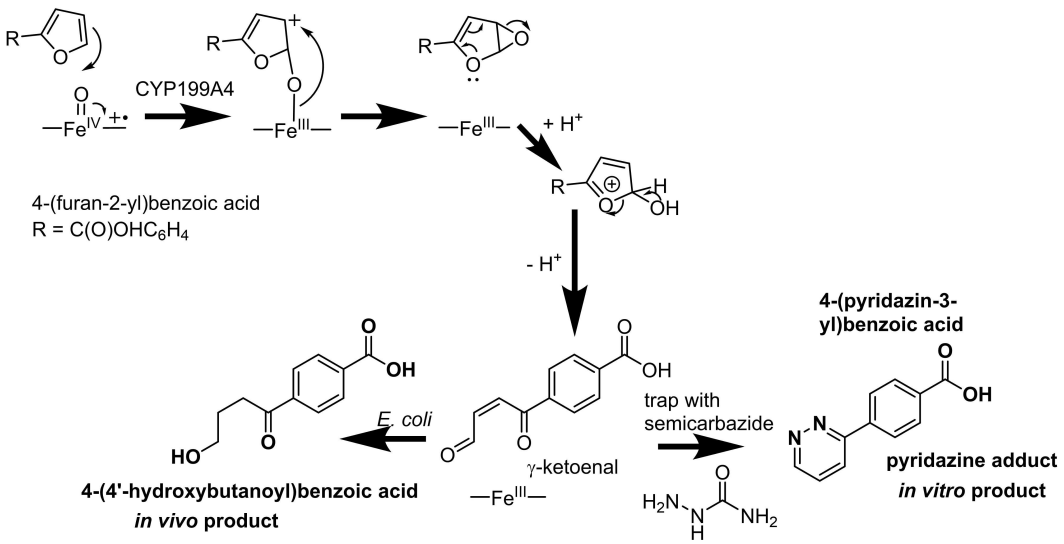

Scheme 2. Potential mechanistic route to the identified (bold) and proposed metabolites of 4-(furan-2-yl)benzoic acid after in vivo and in vitro oxidation by CYP199A4. Alternative mechanisms could include a radical intermediate preceding the cationic species highlighted here or direct formation of the epoxide.

2 compared to the derivatized substrate) could arise from elimination of water or $HOSiMe_3$ from 4-(4′-hydroxybutanoyl)benzoic acid during the sample preparation steps or GC-MS analysis (Figure S7).

As no substrate conversion was observed in the whole-cell oxidation control reactions without CYP199A4 we hypothesize that this metabolite does not arise from reduction of the furan ring by *E. coli* enzymes followed by P450-catalyzed oxidation of a non-aromatic tetrahydro- or dihydro-furan species (Figure S11). Erve and co-workers have identified an equivalent metabolite to the one above from metabolism of the furan ring of prazosin by microsomal cytochrome P450 enzymes.[24] This was proposed to be derived from the P450-catalyzed oxidation of the furan ring to a reactive γ-keto-α,β-unsaturated aldehyde (*cis*-enedial or γ-ketoenal).[4,17c,25] Such a species could be an intermediate on the pathway to the formation of 4-(4′-hydroxybutanoyl)benzoic acid in the whole-cell *E. coli* oxidation systems (Scheme 2). This further processing to 4-(4′-hydroxybutanoyl)benzoic acid could occur through *E. coli* enzymes such as ene reductases.[26] We note that microsomal P450 enzymes have been reported to catalyze the reduction as well as the oxidation of α,β-unsaturated aldehydes.[27]

This γ-ketoenal species is highly electrophilic and is known to react with nucleophiles, including those found in biomolecules, making its identification and analytical quantitation difficult.[25b,28] However, the γ-ketoenal has been trapped with range of species including semicarbazide which can form a pyridazine (Scheme 2).[15c] Therefore, we undertook in vitro CYP199A4-catalyzed oxidations of 4-(furan-2-yl)benzoic acid in the presence of semicarbazide. GC-MS analysis of the reactions after derivatization identified a new metabolite with a mass of 272.2 which is in agreement with the expected mass of the TMS-derivatized 4-(pyridazin-3-yl)benzoic acid (272.1; Scheme 2 and Figure S12).

NMR analysis of the metabolites arising from the in vivo oxidation of the thiophene substrates revealed complex spectra which contained too many ^{13}C signals for a simple hydroxylation, epoxidation or sulfoxidation metabolite (Figures S13–S15). They contained 18 unique carbon signals which would be indicative of dimer formation. Work by Boyd and co-workers demonstrated that non-heme dioxygenase enzymes were capable of catalyzing the sulfoxidation of thiophenes and that the thiophene oxide metabolite would spontaneously dimerize via a Diels-Alder reaction (Scheme 3).[29] Dansette and co-workers also showed that microsomal cytochrome P450 enzymes could catalyze similar sulfoxidation-triggered dimerization reactions alongside aromatic oxidation of the thiophene ring.[18a] We propose that the Diels-Alder dimerization step happens outside of the enzyme active site.

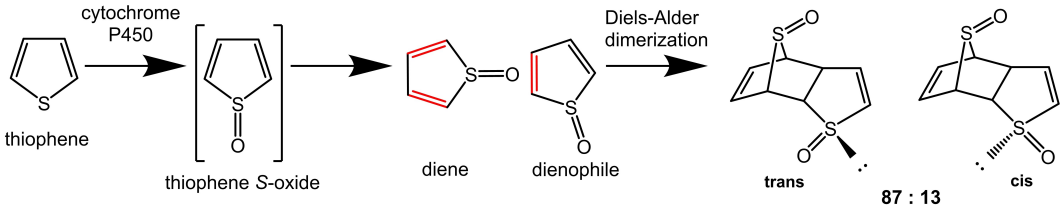

Scheme 3. A general mechanistic scheme for the Diels–Alder dimerization of a thiophene *S*-oxide.[20,30]

The purified metabolites were analyzed by high-resolution mass spectrometry (HRMS) to confirm their identity (Figures S16 and S17). The exact mass of each Diels-Alder dimer is 440.0388 Da. When the 4-(thiophen-3-yl)benzoic acid metabolite was analyzed by HRMS, ions were observed at *m/z* 441.0453 (corresponding to the protonated molecule), *m/z* 458.0789 (NH_4^+ adduct) and *m/z* 463.0287 (Na^+ adduct), in agreement with the product being a Diels-Alder dimer. Similarly, when the 4-(thiophen-2-yl)benzoic acid major and minor products were analyzed by HRMS, ions were observed at 441.0453 or 441.0462 for the protonated molecule, and 463.0264 or 463.0290, corresponding to the Na^+ adduct. The formation of any of these large non-volatile dimeric species would explain why GC-MS analysis of the products from thiophene substrates is difficult. Using this knowledge, we assigned the major metabolites of the CYP199A4-catalyzed oxidations as [4 + 2] Diels-Alder dimers arising from the thiophene oxide species (Scheme 3, Figure 5 and Figures S13–S15).

The major product of 4-(thiophen-2-yl)benzoic acid was assigned as the *trans* stereoisomer (Figure S13) and the minor product formed was designated as the *cis* stereoisomer based on the NMR spectra (Figure S14). In the *trans* isomer, both sulfur atoms have the same absolute configuration, while in the *cis* isomer, the sulfur atoms have opposite absolution configuration. The NMR signals were in broad agreement with those reported by Boyd et al. for the *cis* and *trans* metabolites of 2-phenylthiophene from a dioxygenase enzyme (see Supporting Information, Figures S13 and S14).[29a] Assignment of the stereochemistry of the metabolite of 4-(thiophen-3-yl)benzoic acid was less clear from the NMR based on previous results. It is likely to be the *trans* isomer (Figure S15). The ROESY spectrum indicated that the metabolite arising from the oxidation of 4-(thiophen-3-yl)benzoic acid was the 3,5-substituted dimer, not the 3,6-substituted dimer (Figure S15).

During the oxidation of 4-(thiophen-2-yl)benzoic acid there was also a noticeable change in the color of the reaction mixture (Figure S18). During HPLC purification of the large-scale reaction we observed two additional metabolites which were formed in much lower quantities than the minor product determined above (Figure S19). One of these was brown in color and eluted significantly earlier in the chromatogram. The other eluted at a similar retention time to the thiophene oxide dimers (Figure S19). Neither were produced in large enough quantities to be conclusively identified. Dansette and co-workers found that microsomal P450s could also catalyze arene epoxidation of 2-phenylthiophene resulting in a thiolactone species (Figure S20).[18a] This was unstable and resulted in further oxidation to strongly colored thio-indigo-like compounds (described as being blue to brown) and a similar process may explain the color we observed here.[31] We note that the GC-MS analysis did show a minor metabolite with a mass that would correspond to a tautomer of the thiolactone species described above (trapped by derivatization; Figure S20).

In vitro CYP199A4 reactions with 4-(thiophen-2-yl)- and 4-(thiophen-3-yl)-benzoic acid were also performed in the presence of *N*-methylmaleimide (a dienophile) in an attempt to trap the reactive thiophene *S*-oxide (Scheme 4).[32] New species were detected, and GC-MS analysis was consistent with the expected Diels-Alder adducts (Figure S21).

Density functional theory calculations of the Diels-Alder reactions

Density functional theory (DFT) calculations were performed to understand the observed selectivities of the Diels-Alder reactions. In principle, taking account of all regiochemical and stereochemical variables, there are a total of 64 distinct isomeric transition states (TSs) for the dimerization of each oxide, 4-(1-

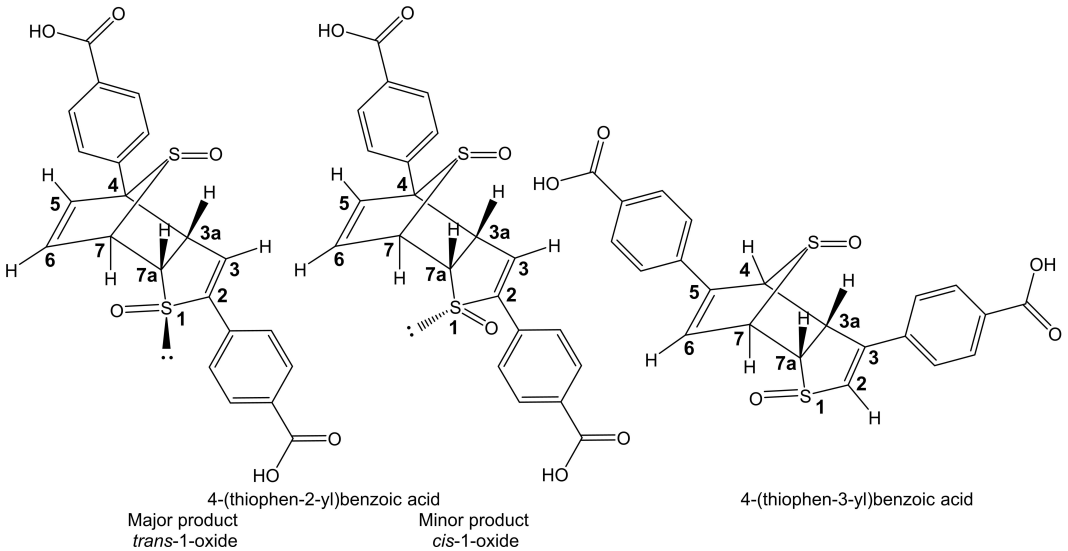

Figure 5. The major and minor metabolites characterized from the CYP199A4-catalyzed oxidation of 4-(thiophen-2-yl)benzoic acid and 4-(thiophen-3-yl)benzoic acid. These products would arise from spontaneous dimerization of the thiophene *S*-oxide metabolites, 4-(1-oxidothiophen-2-yl)benzoic acid and 4-(1-oxidothiophen-3-yl)benzoic acid.

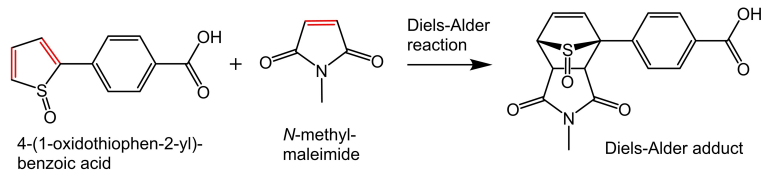

Scheme 4. The unstable thiophene *S*-oxide metabolite, 4-(1-oxidothiophen-2-yl)benzoic acid, was trapped with *N*-methylmaleimide.

oxidothiophen-2-yl)benzoic acid or 4-(1-oxidothiophen-3-yl)benzoic acid. The two lowest-energy TSs for each oxide are shown in Figure 6. A description of the other TSs (which are high in energy and do not contribute significantly to the reactions) is given in the Supporting Information (Table S1 and Figures S22–S27).

The calculations predict that both oxides' TSs share a common preferred arrangement of the reactive core, which can be described as a *syn-syn-endo* arrangement (for a definition of the stereochemical descriptors, see the Supporting Information). This arrangement is also preferred in the dimerization of the parent species, thiophene oxide (see Figure S24). Previous calculations on the Diels-Alder reaction of thiophene oxide with ethylene showed that a *syn* approach by the dienophile (ethylene) with respect to the thiophene oxide was strongly preferred.[34,35] The thiophene oxide has a puckered geometry which is in effect pre-distorted toward *syn* addition. The thiophene oxide dimerizations in Figure 6 mirror this preference but also introduce new selectivity factors. Regiochemically, out of the two C=C bonds in the oxide, there is a preference for the less sterically hindered, unsubstituted C=C bond to serve as the dienophile. Stereochemically, the lowest-energy TS for each oxide has both sulfur atoms in the same absolute configuration (*R*,*R* or *S*,*S*) while the second lowest has the sulfur atoms in opposite configurations (*R*,*S*). Because the absolute configuration and enantiomeric purity of the initially formed thiophene

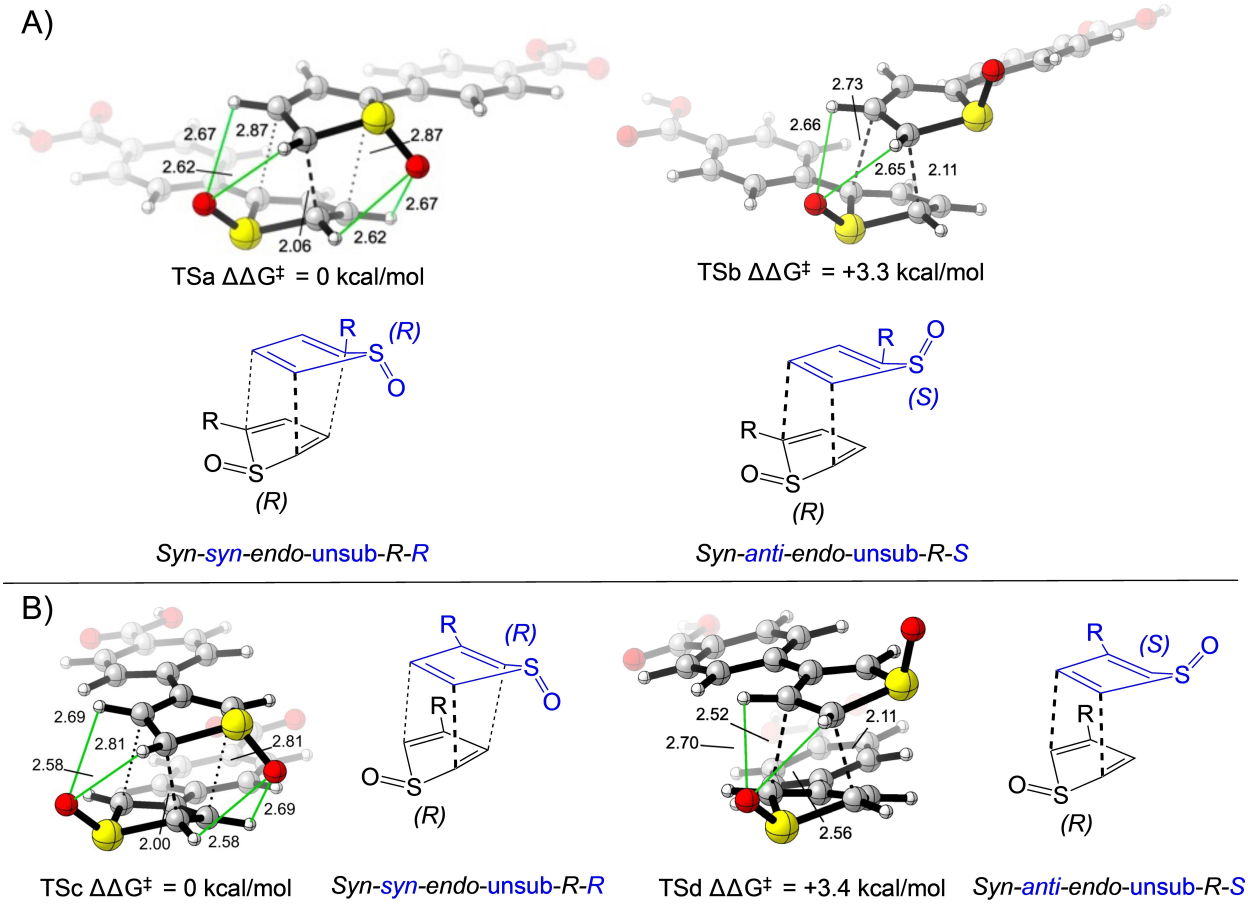

Figure 6. The two most favored transition states for Diels-Alder dimerizations of: A) 4-(1-oxidothiophen-2-yl)benzoic acid, and B) 4-(1-oxidothiophen-3-yl)benzoic acid, computed with M06-2X/def2-TZVPP/SMD(Water)//B3LYP-D3(BJ)/6-31G(d).[33] Distances labeled in Å. Weak CH–O hydrogen bonding is shown by green lines. Forming C–C bonds are indicated as dashed or dotted lines. The dashed lines indicate bonds that can be definitively assigned as forming bonds in each TS. The dotted lines indicate the two equivalent C···C interactions found within the two ambimodal transition states (TSa and TSc); depending on dynamical effects, one of these interactions will go on to form a full bond while the other will not form a bond.

oxides generated by CYP199A4 are not known with certainty, we considered both homodimerization and heterodimerization as mechanistic possibilities here. The calculations predict a strong preference ($\geq$3.3 kcal/mol) for homodimerization. On this basis, we deduce that even if the enzyme produces a mixture of *R* and *S* oxides, the preferred Diels-Alder reaction pathway will still be *R*+*R*, or *S*+*S*, or both, but not *R*+*S*. Assuming (see below) that the thiophene oxide is generated in the *R* configuration, then the *syn-syn-endo*-unsub-*R,R* mode of addition is preferred because it maximizes the stabilizing π–π interactions of the phenyl rings, allows for the sterically less hindered and less resonance-delocalised C=C bond to act as the dienophile, and promotes favorable non-classical CH–O hydrogen bonding interactions between the cycloaddends (Figure 6, green lines). Homodimerization is preferred because it either avoids unfavorable lone pair-π electrostatic interactions between the aromatic substituent and oxygen, in the case of 4-(1-oxidothiophen-2-yl)benzoic acid, or maximizes stabilizing π–π interactions between the aromatic substituents, in the case of 4-(1-oxidothiophen-3-yl)benzoic acid. For further discussion of these effects, see the Supporting Information.

For each oxide, the preferred transition state has C_2 symmetry and is ambimodal.[36] The TS contains three partially-developed C–C interactions: one short interaction (2.06 Å in **TSa**, 2.00 Å in **TSc**) and two longer interactions (2.87 Å in **TSa**, 2.81 Å in **TSc**) (Figure 6). The short interaction and one of the longer interactions will lead to the formation of the two new C–C bonds in the cycloadduct, while the remaining long interaction does not lead to bond formation. It is impossible to tell from the C_2 TS geometry alone which molecule of reactant is acting as the diene and which is the dienophile. Ultimately, both possibilities lead to identical products for a given oxide. Which molecule of oxide is acting as the diene and which is acting as the dienophile in a given instance of the reaction depends on dynamical effects. In order to explore these effects, we performed quasiclassical molecular dynamics trajectory simulations on transition state **TSc** (Figure S27). An investigation comprising 50 simulations showed that one molecule of the oxide acted as the diene in 46% of the trajectories, while the other molecule of oxide acted as the diene in the other 54% of trajectories, within statistical error of the 50:50 ratio expected for an ambimodal TS with C_2 symmetry.

For both thiophene oxides, the calculations predict a strong preference for homodimerization ($\Delta\Delta G^{\ddagger} \geq 3.3$ kcal/mol). The exact selectivities (homodimerization relative to heterodimerization) would depend on the ratio of *R* and *S* thiophene oxides initially generated by the enzyme, but are generally greater than 200:1 at the experimental temperature of 30 °C. The degree of selectivity predicted by theory agrees well with experiment for 4-(1-oxidothiophen-3-yl)benzoic acid, where a single Diels-Alder cycloadduct was obtained. For 4-(1-oxidothiophen-2-yl)benzoic acid, a mixture of two cycloadducts was obtained experimentally. Exploration of several other theoretical methods (Table S2) showed that the selectivity was mildly dependent on the level of theory used; for example, calculations with B2PLYP-D3/def2-TZVPP/SMD(Water)//M06-2X/6-311G(d,p)/SMD(Water) predicted that the energy gaps between the major and minor transition states decreased to 2.3 and 1.9 kcal/mol for the 2- and 3- substituted oxides, corresponding to a selectivity of 50:1 and 20:1, respectively. As the relative ordering of the transition states was not affected, and the selectivities were relatively insensitive to the level of theory used (**TSa** and **TSc** always being favored relative to their respective minor TSs by at least 2 kcal/mol), we conclude that other factors that are not modeled in the calculations must be responsible for the formation of the minor product in the reaction of 4-(1-oxidothiophen-2-yl)benzoic acid (e.g. specific interactions of the enzyme with the initially-formed thiophene oxide).

Crystal structures of the furan and thiophene substrates bound to CYP199A4

The substrate-bound forms of the CYP199A4 enzyme with all three substrates were crystallized using standard conditions (see experimental section). The structures were determined, and the crystals consisted of a single subunit with $P12_11$ symmetry (Table S3). The overall protein fold in each was similar to the structures of CYP199A4 solved previously and to each other (Figure S28).[21b,22b] In all three structures, the residues that constitute the active site of CYP199A4 were in similar positions to those observed in other structures. The phenylalanine 298 residue, which can move to accommodate substrates with large substituents, was in a similar position to that observed in the 4-phenylbenzoic acid-bound structure (PDB code: 7JW5).[7c,21b] In all the structures there was electron density in the active site that could be modelled as the thiophene or furan substrates (Figure 7 and Figure 8). In each structure, the substrate carboxylate interacts with the side chains of R92, S95 and S244, as well as R243 via an ordered water molecule.

In the crystal structure of CYP199A4 with 4-(furan-2-yl)benzoic acid, electron density which could be ascribed to the substrate was observed. Additional electron density for a heme-bound aqua ligand was also present. The refined occupancies of the substrate and the water molecule were 89% and 83%, respectively. The furan ring of the substrate was assigned as having its oxygen held close to the heme (rather than directed away; Figure S29). This allows the furan oxygen to hydrogen-bond to the heme-bound aqua ligand (O–O distance: 2.9 Å). If the ring were flipped by 180°, there would instead be a steric clash between the furan ring and the heme-bound aqua ligand (W1; Figure S29). The hydrogen bonding interaction between the oxygen atom of the furan ring and the water ligand could explain why the water ligand is not displaced when this substrate binds. This is consistent with the observation that 4-(furan-2-yl)benzoic acid induces only a 35% spin-state shift to the high-spin form when it binds to CYP199A4.

A γ-ketoenal could be formed from electrophilic attack at either of the carbon atoms *ortho* to the furan oxygen (C8 and C11; Scheme 2). One of these (C8) is also substituted with the aromatic ring of the benzoic acid which would have electronic and steric effects on the preference for electrophilic attack. These carbons are 5.4 Å and 4.8 Å from the iron compared to

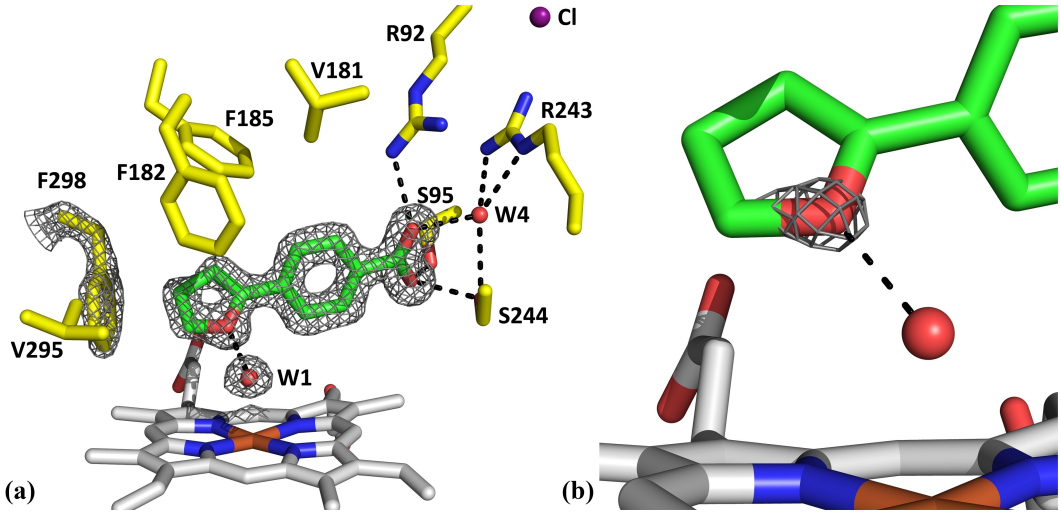

Figure 7. a) Crystal structure of 4-(furan-2-yl)benzoic acid-bound CYP199A4, determined at 1.42-Å resolution (PDB code: 7TRT). In green is the 4-(furan-2-yl)benzoic acid substrate, in yellow are active-site residues, in gray is the heme, and red and purple spheres represent water and chloride, respectively. Dashed black lines represent hydrogen bonds. A *2mFo-DFc* composite omit map (contoured at 1.5 σ) of the substrate, F298 sidechain and heme-bound aqua ligand (W1) is shown as gray mesh. b) Examination of the omit map of the furan ring at the 4 σ level (gray mesh) reveals the position of the oxygen atom.

the furan O atom which is 4.3 Å away (Figure 7, Table S4). Based on the structure we would hypothesize that the substrate may have to alter its position at some point during the catalytic cycle before oxidation could occur.

In the crystal structure of 4-(thiophen-2-yl)benzoic acid-bound CYP199A4, the substrate binds in a similar position to that of 4-(furan-2-yl)benzoic acid. However, there is not a water ligand bound to the heme iron in this structure (Figure 8 and Figure S30). The refinement of the electron density for 4-(thiophen-2-yl)benzoic acid indicated that it was present in multiple conformations in the active site (Figure S31). The thiophene ring could be oriented with the sulfur held either close to or away from the heme. Both conformations of the substrate were modelled, and the occupancy of each was refined. The occupancy of the conformation in which the sulfur is held closer to the heme was refined to 83% (Figure S31). The alternative conformation in which the sulfur is held away from the heme had an occupancy of only 8%. The observation that this substrate has expelled the heme-bound aqua ligand is in agreement with the larger (75%) type I spin-state shift to HS compared to 4-(furan-2-yl)benzoic acid.

In the 4-(furan-2-yl)benzoic acid crystal structure, in which the heme iron is six-coordinate and low-spin, the iron is roughly in the plane of the porphyrin macrocycle (Figure S29). In the 4-(thiophen-2-yl)- and 4-(thiophen-3-yl)-benzoic acid structures, in which the heme-bound aqua ligand has been removed and the iron is high-spin, the heme iron has moved further below the heme plane. Importantly the structures demonstrate there is only enough space for one substrate molecule to bind within the CYP199A4 active site. This would suggest that the dimerization reactions occurs when the product leaves the active site. In the crystal structure, the sulfur of the 4-(thiophen-2-yl)benzoic acid ring is located 4.2 Å from the heme iron. The closest carbon (C_{12}) of the thiophene ring in the major conformation was 5.3 Å from the iron (refer to Table S5 for the numbering scheme). When coupled with the relative energetic ease of sulfoxidation compared to aromatic oxidation this could explain the observed activity (Table S5).[37]

The crystal structure of 4-(thiophen-3-yl)benzoic acid-bound CYP199A4 was very similar to that of 4-(thiophen-2-yl)benzoic acid (Figure 8). There were some minor changes within the active site in the orientation of the threonine 395 residue and the presence of an additional water molecule nearby (Figure S32). In the structure the orientation of the sulfur in the thiophenyl moiety of 4-(thiophen-3-yl)benzoic acid was determined by examining the electron density map at the 3 σ level, which revealed a region of higher electron density corresponding to the position of the sulfur atom (Figure 8). The thiophenyl ring Cβ is 4.2 Å from the iron with the sulfur atom being 5.2 Å from the iron. When the Cpd I oxygen was modeled 1.62 Å from the heme iron, the distances from the oxygen atom to the thiophene ring were Cα–O, 4.0 Å; Cβ–O, 2.9 Å and S–O, 4.1 Å, respectively (Table S5). The angles of the Fe=O to the substrate for the thiophene ring atoms of 4-(thiophen-3-yl)benzoic acid were Cα, 143.8°; Cβ, 135.1° and S, 123.8°, respectively. Despite the closer distance of the carbon atoms to Fe=O, the major metabolite arose from sulfoxidation highlighting that this must be the energetically more favorable reaction. At this stage we cannot rule out that there may also be conformational changes in the enzyme, which enables movement of the substrate from this position, during the catalytic cycle.

In the 4-(thiophen-3-yl)benzoic acid structure, the sulfur is held further from the heme iron (5.2 Å) than in the structure with 4-(thiophen-2-yl)benzoic acid (4.2 Å). When the oxygen of Cpd I is modeled above the heme, the sulfur of 4-(thiophen-3-yl)benzoic acid is 4.1 Å from the Cpd I oxygen, while the sulfur of 4-(thiophen-2-yl)benzoic acid is 2.9 Å from the oxygen of Cpd I. This longer distance along with the approach angle (the Fe=O–S angles are 123.8° for 4-(thiophen-3-ylbenzoic acid and 135.8° for 4-(thiophen-2-yl)benzoic acid) are consistent with the

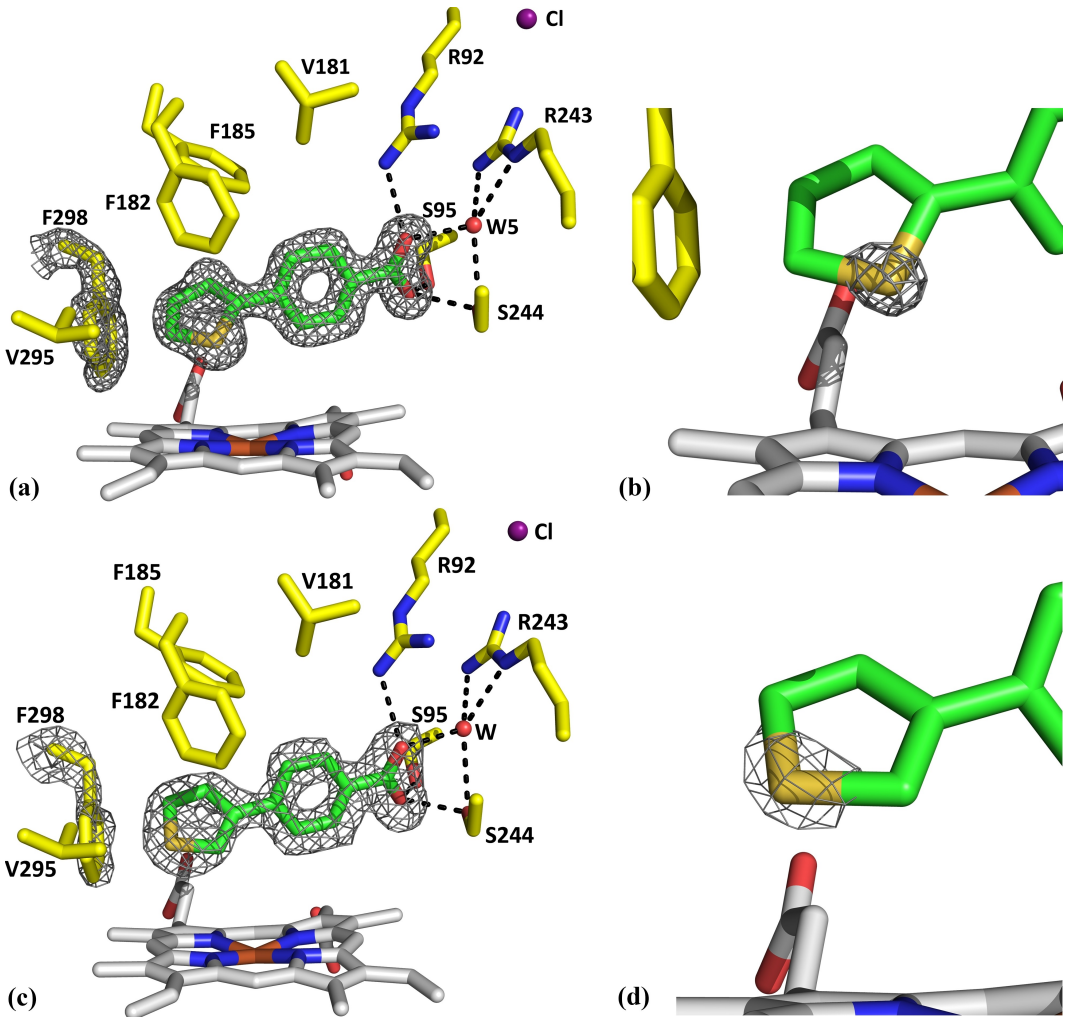

Figure 8. a) Crystal structure of 4-(thiophen-2-yl)benzoic acid-bound CYP199A4, determined at 1.45-Å resolution (PDB code: 7TRU). In green is the 4-(thiophen-2-yl)benzoic acid substrate, in yellow are active-site residues, in gray is the heme, and red and purple spheres represent water and chloride, respectively. Dashed black lines represent hydrogen bonds. A *2mFo-DFc* composite omit map (contoured at 1.5 σ) of the substrate and F298 sidechain is shown as gray mesh. b) The position of the sulfur in the five-membered ring was deduced based on the higher electron density at this position. The composite omit map of the substrate (gray mesh) has been contoured at 6 σ to show the higher electron density at this position of the ring. c) The crystal structure of 4-(thiophen-3-yl)benzoic acid-bound CYP199A4, determined at 1.66-Å resolution (PDB code: 6C3J). The substrate is depicted in green, the heme in gray, active-site residues in yellow and waters (W) as red spheres. A *2mFo-DFc* composite omit map (contoured at 1.0 σ) of the substrate and F298 side chain is shown as gray mesh. F298 has been displaced to accommodate the thiophene moiety. d) The composite omit map contoured at 3 σ reveals the position of the sulfur atom in the heterocyclic ring.

lower activity and reduced levels of P450 oxidation metabolites with this substrate compared to the 4-(thiophen-2-yl)benzoic acid isomer.

The binding orientations observed in the substrate-bound crystal structures (Figure 8) suggest that the oxidations of both thiophene substrates would preferably yield the *R* enantiomer of the oxides. This would favor the formation of the *R*,*R* homodimers based on the calculations on the Diels-Alder reaction (Figure 6).

Conclusions

Two thiophenes – 4-(thiophen-2-yl)benzoic acid and 4-(thiophen-3-yl)benzoic acid – were metabolized by CYP199A4 almost exclusively via sulfoxidation. There was some evidence of alternative oxidative metabolites with 4-(thiophen-2-yl)benzoic acid, with other minor colored products observed. These minor metabolites may arise from aromatic ring oxidation from an alternative orientation of the thiophene moiety of the substrate in which the sulfur points away from the heme, for which there is evidence from the crystal structure. After sulfoxidation the thiophene oxide rings were activated towards Diels-Alder dimerization. Calculations were in agreement with the experimental data in predicting a strong preference for the formation of a single major product from each thiophene; the computations predict that in each case the product would arise from homodimerization of one enantiomer of the thiophene oxide. Based on the crystal structures this is predicted to be the *R* enantiomers of the oxides, leading to *syn-syn-endo-R,R* dimers.

In whole-cell oxidation reactions, all the 4-(thiophen-2-yl)benzoic acid added to the reaction (4 mM) was consumed. CYP199A4 had lower activity towards 4-(thiophen-3-yl)benzoic acid with significantly less of the oxidized metabolite being generated. This was in agreement with the structural information which demonstrated that the sulfur of the thiophene ligand in 4-(thiophen-2-yl)benzoic acid was better placed in relation to the heme and the reactive intermediate for the sulfoxidation reaction to occur. The sulfoxide (thiophene oxide) dimer was still the major product with 4-(thiophen-3-yl)benzoic acid despite the longer distance of the sulfur to the heme, and despite the fact that a carbon atom of this substrate was located closer to the heme. Overall, this highlights the preference cytochrome P450 enzymes have for sulfoxidation over aromatic hydroxylation.

Replacing the sulfur with an oxygen in the aromatic system resulted in different P450-catalyzed activity with CYP199A4. 4-(Furan-2-yl)benzoic acid was oxidized to a highly reactive γ-keto-α,β-unsaturated aldehyde (*cis*-enedial or γ-ketoenal) species. This could not be characterized directly due to its reactivity but could be trapped in vitro using semicarbazide to generate a pyridazine species. In whole-cell oxidation systems it was further processed to 4-(4′-hydroxybutanoyl)benzoic acid, potentially by *E. coli* enzymes such as an ene reductase. However, it should be noted that microsomal P450 enzymes have been reported to catalyze the reduction of α,β-unsaturated aldehydes.[27] Furan ring systems are more pi excessive than thiophenes or benzenes and this may enable electrophilic attack of the Cpd I intermediate on the aromatic ring to be more feasible for the CYP199A4 enzyme compared to the phenyl ring of 4-phenylbenzoic acid. The latter does not obtain an optimal position for aromatic oxidation within the active site of the CYP199A4 enzyme.

Experimental Section

Abbreviations used: BA, benzoic acid; MeCN, acetonitrile; DFT, density functional theory; DMSO, dimethyl sulfoxide; EMM, *Escherichia coli* minimal media; EtOH, ethanol; BSTFA, *N,O*-Bis(trimethylsilyl) trifluoroacetamide; TMCS, trimethylchlorosilane; TFA, trifluoroacetic acid; GC-MS, gas chromatography-mass spectrometry; HRMS (high-resolution mass spectrometry); LB, Luria Bertani Broth; IPTG, Isopropyl β-D-1-thiogalactopyranoside; NADH, reduced nicotinamide adenine dinucleotide; TS, transition state; TO, thiophene oxide; TO2, 4-(1-oxidothiophen-2-yl)benzoic acid; TO3, 4-(1-oxidothiophen-3-yl)benzoic acid; Tris, tris(hydroxymethyl)aminomethane. PDB, Protein Data Bank (http://www.rcsb.org/); Bis-Tris, 2,2-Bis(hydroxymethyl)-2,2′,2′′-nitrilotriethanol; PEG, polyethylene glycol.

General: 4-(Thiophen-2-yl)-, 4-(thiophen-3-yl)- and 4-(furan-2-yl)-benzoic acid were purchased from Fluorochem Ltd. Semicarbazide hydrochloride were from Sigma-Aldrich. BSTFA + TMCS (99 : 1) was from Supelco. Analytical high-performance liquid chromatography (HPLC) was performed using a Kinetex XB-C18 reversed-phase liquid chromatography column (100 Å pore size, 250 × 4.6 mm, 5 μm; Phenomenex). The instrument used for analytical HPLC was a Shimadzu Prominence LC-20AD Liquid Chromatograph, with a DGU-20 A_{5R} degassing unit, SIL-20 A autosampler, CTO-20 A column oven, and SPD-20 A UV/Vis Detector. A gradient of 20%–95% v/v MeCN in H_2O (with 0.1% v/v TFA) was used to elute the samples at a rate of 1 mL min^{-1}. The eluate was monitored at 254 nm. A preparative-scale Kinetex EVO C18 AXIA Packed reversed-phase column (100 Å pore size, 150 × 21.2 mm, 5 μm; Phenomenex) was used to purify the products of the in vivo CYP199A4 reactions. Prep-scale HPLC was performed using a Shimadzu LC-20AR Liquid Chromatograph, equipped with a DGU-20 A_{5R} degassing unit, a SIL-20AC HT autosampler, CTO-20AC column oven, CMB-20 A system controller, and SPD-M20 A photo-diode array detector. Media composition per L; LB broth; Sodium chloride (5 g), Bacto yeast extract (5 g), Bacto tryptone (10 g); Trace Elements; Na_2EDTA (20.1 g), $FeCl_3.6H_2O$ (16.7 g), $CaCl_2.H_2O$ (0.74 g), $CoCl_2.6H_2O$ (0.25 g), $ZnSO_4.7H_2O$ (0.18 g), $MnSO_4.4H_2O$ (0.132 g), $CuSO_4.5H_2O$ (0.10 g); EMM (*E. coli* minimal media) K_2HPO_4 (7 g), KH_2PO_4 (3 g), $(NH_4)_2SO_4$ (1 g), $Na_3Citrate$ (0.5 g), $MgSO_4$ (0.1 g), 20 mL of 20% glucose (the $MgSO_4$ and glucose was added after the salt solution had been autoclaved and immediately before use.).

Production and purification of CYP199A4, HaPux and HaPuR: Wild-type CYP199A4 was produced and purified according to the published procedure.[14b] Ferredoxin (HaPux) and ferredoxin reductase (HaPuR) were prepared as described previously.[22a] Proteins were stored at −20 °C in ~50% glycerol. Glycerol was removed prior to use using a PD-10 desalting column (Cytiva).

Spin-state shift and binding affinity analysis: Spin-state shifts induced by the binding of substrates to CYP199A4 and the substrate binding affinity (K_d values) were measured according to the published procedures.[21a] All the binding affinities were determined using the Morrison tight binding equation (the concentration of the enzyme ranged from 2.5 to 2.9 μM).[38]

In vitro NADH activity assays: In vitro reactions were performed on a 1.2-mL scale at 30 °C and contained 5 μM HaPux, 0.5 μM CYP199A4, 0.25 μM HaPuR and 100 μg mL^{-1} bovine liver catalase in oxygenated Tris-HCl buffer (50 mM, pH 7.4). Reaction mixtures were incubated at 30 °C for 2 min prior to addition of NADH (~320 μM). Substrate (1 mM) was subsequently added from a 100 mM stock solution to initiate each reaction. The solvent for the stock solutions was DMSO for both the thiophenes and a 50 : 50 mixture of DMSO/EtOH for the furan. NADH consumption was monitored at 340 nm using an extinction coefficient of $\varepsilon_{340} = 6.22$ mM^{-1} cm^{-1}.[39] NADH consumption rates (*N*) are reported in units of μM μM(P450)$^{-1}$ min^{-1} (abbreviated to min^{-1}) and were calculated from the slope of the plot of absorbance against time ($\Delta A_{340}/\Delta t$) using the equation:

$$N = \frac{\frac{\Delta A_{340}}{\Delta t} \times 1000}{6.22\ \text{mM}^{-1}\text{cm}^{-1} \times [\text{P450}]}$$

(the linear portion of the plot was used when measuring the slope). The NADH leak rate in the absence of substrate was ~9 min^{-1}. Note that the leak rate was not subtracted from measured NADH consumption rates. The rate of NADH consumption by CYP199A4 with 4-(thiophen-3-yl)benzoic acid was slow and therefore the consumption of NADH was only monitored for the first 20 min, and the reaction mixture was then left at room temperature for a further 2 h to ensure that all NADH was consumed.

Analysis of metabolites: In vitro reaction mixtures were prepared for HPLC analysis by mixing 132 μL of the reaction mixture with 66 μL of acetonitrile and 2 μL of internal standard (10 mM 9-hydroxyfluorene in EtOH) and the samples were centrifuged to remove particulate matter. A 20–95% gradient of MeCN in H_2O (with 0.1% TFA) was used to elute the sample. The eluate was monitored at 254 nm (0.2% TFA was added to the HPLC samples from whole-cell oxidation reactions as peak splitting occurred if less acid was added).

Gas chromatography experiments were performed on a Shimadzu GC-17 A with a QP5050 A GC-MS detector, equipped with a DB-5 MS fused silica column (30 m × 0.25 mm, 0.25 μm). The injector was held at 250 °C and the interface was 280 °C. The column temperature was held at 120 °C for 3 min and then increased at 6 °C min^{-1} until it reached 230 °C. The column was held at this temperature for 6 min. Alternatively the samples were analyzed using a Shimadzu GC-2010 with a GCMS-QP2010S detector, using a DB-5 MS column (30 m × 0.25 mm, 0.25 μm). The injection temperature was 250 °C and the interface temperature was 280 °C. The column was held at 120 °C for 3 min and was then raised at a rate of 7.5 °C min^{-1} to 240 °C, and the temperature was held at 240 °C for 1 min. The temperature was then increased to 250 °C at a rate of 2 °C min^{-1} and held at 250 °C for 5 min. Peak integrations were determined using the total ion count.

Trapping of the ring-opened furan metabolite with semicarbazide: Erve et al. reported that the reactive γ-ketoenal arising from P450-catalyzed ring-opening of a furan ring could be trapped with semicarbazide (giving a pyridazine product).[24b] In vitro CYP199A4 reactions with 4-(furan-2-yl)benzoic acid were performed in the presence of 1 mM semicarbazide to trap the γ-ketoenal intermediate. Reactions were performed according to the procedure for "in vitro *NADH activity assays*" described above. Semicarbazide hydrochloride (1 mM) was added from a 100 mM stock solution in Milli-Q water either at the start of the reaction (immediately after addition of the 4-(furan-2-yl)benzoic acid substrate), or at the end of the reaction once all of the NADH had been consumed. Control reactions were also performed which either lacked the P450 or lacked the semicarbazide. The in vitro reactions were analyzed by HPLC and GC-MS. For GC-MS analysis, 900 μL of the reaction mixture was acidified with 3 μL of 3 M HCl, followed by extraction with 3 × 400 μL ethyl acetate. The combined organic extracts were dried with anhydrous $MgSO_4$, and the solvent evaporated under N_2 gas. The residue was re-dissolved in 150 μL of anhydrous MeCN and derivatized with > 35 μL of BSTFA + TCMS (99 : 1). The samples were incubated at 37 °C for 2 h before GC-MS analysis.

Trapping of the thiophene S-oxide metabolites with N-methylmaleimide: In vitro CYP199A4 reactions with 4-(thiophen-2-yl)benzoic acid and 4-(thiophen-3-yl)benzoic acid were performed in the presence of *N*-methylmaleimide. Reactions (1.2 mL) contained 5 μM HaPux, 0.25 μM HaPuR, 0.5 μM CYP199A4 and ~1 mM *N*-methylmaleimide (from a 100 mM stock solution in EtOH) in Tris buffer (50 mM, pH 7.4). Reactions were initiated by addition of ~320 μM NADH followed by ~1 mM 4-(thiophen-2-yl)benzoic acid or 4-(thiophen-3-yl)benzoic acid (from a 100 mM stock solution in DMSO). Control reactions omitting the P450 enzyme (but containing all other reaction components, including *N*-methylmaleimide), were also performed. Reactions were prepared for HPLC and GC-MS analysis as described above.

In vivo (whole-cell) activity assays: A pETDuet plasmid harboring HaPux and HaPuR genes and a pRSFDuet vector harboring HaPux and wild-type CYP199A4 genes were transformed into BL21 (DE3) competent *E. coli* cells (New England Biolabs). A 600 mL volume of LB broth containing 30 mg L^{-1} kanamycin and 100 mg L^{-1} ampicillin was inoculated with a single colony of bacteria. The bacteria were incubated at 37 °C and 140 rpm for ~8 h and the temperature was then reduced to 18 °C. Benzyl alcohol (0.02 % v/v), EtOH (2 % v/v) and trace elements solution (2.4 mL) were subsequently added. After 30 min, 60 μL of 0.5 M IPTG was added and the mixture was incubated overnight at 18 °C and 105 rpm for ~17 h. The cell mixture was centrifuged (5000 g, 10 min) to harvest the cell pellet and the pellet was resuspended in 600 mL of EMM. For each substrate tested, a 150 mL aliquot of the *E. coli* mixture was transferred into a 2-L baffled flask and the reactions were initiated by addition of 2 mM substrate. The substrates tested were 4-(furan-2-yl)-, 4-(thiophen-2-yl)- and 4-(thiophen-3-yl)-benzoic acid. The reactions were incubated at 30 °C and 150 rpm for 24 h. After 4 h, an additional 2 mM of substrate was added to each reaction. Reaction progress was monitored by HPLC. After 2 and 22 h, 1 mL aliquots of the reaction mixture were removed and centrifuged to eliminate the cell pellet (6000 rpm, 10 min). To 132 μL of the supernatant was added 66 μL of acetonitrile and 2 μL of internal standard (10 mM 9-hydroxyfluorene in EtOH). Each solution was centrifuged again to remove any precipitate, acidified with 0.2 % v/v TFA and analyzed by HPLC. Control reactions were performed with an empty pRSFDuet vector (harboring a kanamycin-resistance gene) in BL21 (DE3) *E. coli* cells.

After 24 h, the cell debris was removed from the whole-cell reaction mixtures by centrifugation (5000 g, 15 min). The cell pellet was re-suspended in EMM (50 mL) and centrifuged again to remove the cell debris. The supernatant from the two centrifugation steps was combined and freeze-dried for ~64 h. The freeze-dried samples were stored at −20 °C for later purification of the P450 metabolites.

No reaction products or substrate was observed in the supernatant of the whole cells oxidation of 4-(thiophen-3-yl)benzoic acid. A white precipitate was observed along with the cell pellet after centrifugation. The reaction was performed again on a 200-mL scale, with 2 mM substrate for 24 h. The cell pellet and white precipitate were re-dissolved in a mixture of Tris buffer (10 mL), MeCN (10 mL), EMM (7 mL) and DMSO (8 mL). The mixture was centrifuged again to remove the cell pellet. The cell pellet was washed with Tris buffer (2 mL) and DMSO (2 mL) and centrifuged. The supernatant from each centrifugation step was combined, the acetonitrile was removed under N_2 gas, and the solution was freeze-dried for ~48 h.

Purification of the in vivo CYP199A4 reaction products

4-(Thiophen-2-yl)benzoic acid: A portion of the freeze-dried crude product was re-dissolved in a mixture of 50 mM Tris buffer, pH 7.4 (5.4 mL), MeCN (2.6 mL) and acidified with 16 μL of TFA. The mixture was centrifuged to remove particulate matter (6000 rpm, 2 min). A preparative-scale Kinetex EVO C18 AXIA Packed reversed-phase column (100 Å pore size, 150 × 21.2 mm, 5 μm; Phenomenex) was used to purify the P450 product. The gradient was 20–31 % MeCN in Milli-Q water (0.2 % TFA) over 25 min and the flow rate was 5 mL min^{-1}. The HPLC sample was directly acidified with ~0.1 % TFA prior to injection to prevent split peaks. The fractions containing the major product and most abundant minor product were collected, the MeCN was evaporated under N_2 gas, and the solutions were freeze-dried for ~48 h. The major product was a white powder.

4-(Thiophen-3-yl)benzoic acid: A portion of the freeze-dried crude product was re-dissolved in a mixture of DMSO (5 mL), MeCN (1.5 mL), Tris buffer (1.5 mL) and acidified with 4 μL of TFA. The mixture was centrifuged to remove particulate matter (6000 rpm, 4 min). A preparative-scale Kinetex EVO C18 AXIA Packed reversed-phase column (100 Å pore size, 150 × 21.2 mm, 5 μm; Phenomenex) was used to purify the P450 product. The gradient was 20–31 % MeCN in Milli-Q water (0.3 % TFA) over 25 min and the flow rate was 5 mL min^{-1}. The HPLC sample was directly acidified with ~1 % TFA prior to injection to prevent split peaks. The fractions containing the major product were combined, the MeCN was evaporated under N_2 gas, and solution was freeze-dried overnight. The purified product was a yellow powder.

4-(Furan-2-yl)benzoic acid: Approximately 1/3 of the freeze-dried product was re-dissolved in Tris buffer (3.5 mL) and MeCN (1.5 mL). The mixture was centrifuged (6000 rpm, 3 min) to remove particulate matter/precipitate. The major product was purified via

preparative-scale HPLC using a gradient of 20–50% MeCN in H_2O (0.1% TFA) over 25 min and a flow rate of 5 mL min^{-1}. The fractions containing the major product were combined, the MeCN was evaporated under N_2 gas, and the solution was freeze-dried. The purified metabolites were characterized via NMR spectroscopy and high-resolution mass spectrometry.

NMR spectroscopy: The structures of the reaction products were elucidated using ^{1}H, ^{13}C, COSY, HMBC, HSQC and ROESY experiments. An Agilent DD2 NMR spectrometer operating at 500 MHz for ^{1}H and 126 MHz for ^{13}C was used to obtain the NMR spectra. NMR spectra were measured in d_6-DMSO.

Energy-minimized 3D models of the Diels–Alder dimers were generated with Chem3D Pro 12.0 using the MM2 force field calculation method (CambridgeSoft). These models were used to verify that the proposed products were consistent with the ROESY spectra.

Control reactions of 4-(thiophen-2-yl)benzoic acid and 4-(thiophen-3-yl)benzoic acid with H_2O_2: Control reactions were performed to demonstrate that the thiophene oxidation products arose from P450-catalyzed oxidation, and not from a reaction with hydrogen peroxide generated via uncoupling.[40] Reactions were performed on a 1.2-mL scale and contained 1 mM 4-(thiophen-2-yl)benzoic acid or 4-(thiophen-3-yl)benzoic acid (from a 100 mM stock solution in DMSO) and 1 or 10 mM H_2O_2 in Tris buffer (50 mM, pH 7.4). The reaction mixtures were incubated at room temperature for 3.5 h.

Reactions were also performed using a higher H_2O_2 concentration (3.3 M H_2O_2). To a solution of 4-(thiophen-2-yl)benzoic acid or 4-(thiophen-3-yl)benzoic acid (2 mM) in 1 mL of Tris buffer (50 mM, pH 7.4), 0.5 mL of 30% w/w H_2O_2 (~9.8 M) was added. The reaction mixtures were incubated at 37 °C for 4 h. After completion, the reactions were quenched by addition of 6×10 μL aliquots of 10 mg mL^{-1} bovine catalase solution on ice. The samples were prepared for HPLC analysis as described above.

High-resolution mass spectrometry (HRMS): The mass spectrum of the purified in vivo oxidation product was obtained using a 1260 LC system coupled to a 6230 TOF mass spectrometer (Agilent Technologies). Approximately 1 mg of the purified product was dissolved in 1 mL of DMSO. A 10 μL aliquot of this stock solution was then diluted 100-fold in methanol. Sample (10 μL) was directly injected in 50% v/v aqueous acetonitrile (with 0.1% v/v formic acid) at a flow rate of 0.2 mL min^{-1} and ionized via electrospray ionization. No chromatography column was used. The instrument settings were: positive ion mode, mass range of 100–800 *m/z*, capillary voltage 3.5 kV, nozzle voltage 1 kV, gas temperature of 250 °C. Data analysis was performed using MassHunter software (vB.07.00, Agilent Technologies). The chemical formula of the expected product was used to search for each compound, including any H, ammonium or Na adducts.

GC-MS analysis of the purified product of 4-(furan-2-yl)benzoic acid oxidation: The purified product of the in vivo CYP199A4 reaction with 4-(furan-2-yl)benzoic acid was analyzed by GC-MS. A 20 μL aliquot of the purified product dissolved in DMSO was added to 1 mL of ethyl acetate and dried over anhydrous $MgSO_4$. The ethyl acetate was evaporated under a stream of N_2 gas, and the residue was re-dissolved in 150 μL of anhydrous acetonitrile. Derivatization reagent (25 μL of BSTFA + TMCS (99:1)) was added and the sample was incubated at 37 °C for 2 h before analysis using a Shimadzu GC-2010 with a GCMS-QP2010S detector, using the column and method described above.

Density functional theory calculations: Calculations were carried out at the M06-2X/def2-TZVPP/SMD(Water)//B3LYP-D3(BJ)/6-31G(d)[33] level using Gaussian 16 Rev C.01[41] with standard state correction. Initial TS structures were built manually. For the lowest-energy TSs, conformer sampling was performed to check that the carboxylic acid group was in its most stable conformation. Quasiclassical direct dynamics calculations at the B3LYP-D3(BJ)/6-31G(d)[33] level using Gaussian 16 Rev C.01[41] were performed with MILO v1.0.3[42] with default settings.

X-ray crystallography: Purified CYP199A4 (purity ratio: $Abs_{419}/Abs_{280} = 2.1$) was desalted using a PD-10 desalting column (GE Healthcare) and concentrated to ~40 mg mL^{-1} (~900 μM) via ultrafiltration. To the concentrated protein was added 3–4 mM substrate from a 100-mM stock solution in DMSO. The protein-ligand complex was crystallized via the hanging-drop vapour-diffusion method; 1.2 μL of protein was combined with an equal volume of crystallization reagent and the drop was equilibrated against a 500 μL reservoir of crystallization reagent at 16 °C. The crystallization conditions used were those optimized for CYP199A4 previously:[21b,c] 100 mM Bis-Tris buffer (adjusted to pH 5.0–5.75 with acetic acid), 0.2 M magnesium acetate and 20–32% PEG 3350. Clusters of plate-like crystals typically appeared within 24 h.

Crystals were cryoprotected by immersion in Parabar 10312 (Hampton Research) or NVH Immersion Oil (Cargille Laboratories) and mounted onto MiTeGen MicroLoops or MicroMounts and flash cooled in liquid N_2. X-ray diffraction data were collected at 100 K on the MX1 or MX2 beamline at the Australian Synchrotron[43] using 0.9537-Å X-rays. For the crystals of CYP199A4 bound to 4-(furan-2-yl)benzoic acid and 4-(thiophen-2-yl)benzoic acid, automatic data processing was carried out at the Australian Synchrotron using *xdsme*[44] and Aimless.[45] For the 4-(thiophen-3-yl)benzoic acid crystal structure, the data were indexed and integrated using iMosflm[46] and scaling and merging were performed with Aimless.[45] The program PhaserMR was used to solve the phase problem by the molecular replacement method.[47] The structures of CYP199A4 bound to 4-cyclopropylbenzoic acid (PDB code: 5UVB) or 4-methoxybenzoic acid (PDB code: 4DO1) were used as the initial search models (with water molecules and ligands removed). Following molecular replacement, each model was manually adjusted in Coot[48] and the substrate was modeled into positive difference electron density in the active site. Ligand coordinates and restraints were generated using Phenix eLBOW (electronic Ligand Builder and Optimization Workbench).[49] Positive density in the anion binding site was modeled as a chloride ion.[22b] Structure refinement was performed using Phenix.refine, with automatic addition of solvent.[50] If a heme-bound aqua ligand was present, its occupancy was refined. The position of the sulfur/oxygen atom of the substrate's five-membered ring was determined by examining the electron density map at a higher contour level. This revealed a position of higher electron density corresponding to the sulfur/oxygen atom. The orientation of the thiophene/furan ring of the substrate was also deduced by considering hydrogen-bonding interactions with surrounding water molecules. Metal-ligand bond lengths (Fe–O and Fe–S) were not restrained during refinement. *MolProbity* was used for crystal structure validation[51] and fully refined structures were deposited into the Protein Data Bank (PDB) (http://www.rcsb.org/). The PDB codes are 6C3J, 7TRU and 7TRT (Table S3). Feature-enhanced maps,[52] composite omit maps[53] and Polder omit maps[54] were subsequently obtained and figures of the active site were generated using PyMOL.[55]

Crystal structure analysis: Crystal structure analysis was performed with Coot,[48] UCSF Chimera[56] and PyMOL.[55] Studies have calculated the Fe–O bond length of Compound I to be 1.62 Å and measured it as 1.67 Å.[6b,57] Therefore, the ferryl oxygen of Cpd I was modeled 1.62 Å above the heme (along the Fe–S axis) in PyMOL using the script downloaded from https://pymolwiki.org/index.php/CreateAtom. Distances and angles were measured from the

substrate to the Cpd I oxygen to rationalize the regioselectivity of the enzyme.

Supporting Information

The authors have cited additional references within the Supporting Information.[58–64]

Acknowledgements

This research was funded in part by the Autralian Research Council grants DP180103047 (to E.H.K.) and DP140103229 (to S.G.B. and J.J.D.V.). This research was undertaken in part using the MX1 and MX2 beamlines at the Australian Synchrotron, part of ANSTO, and made use of the Australian Cancer Research Foundation (ACRF) detector. The authors also acknowledge the award of an Australian Government Research Training Program Scholarship to T.C. and M.N.P. (PhD). M.N.P. thanks the University of Adelaide for a Constance Fraser PhD Scholarship. This research was supported by an AINSE Ltd. Postgraduate Research Award (PGRA) to M.N.P. Angus Keto is supported by an Australian Government Research Training Program Scholarship and an American Australian Association Graduate Education Fund Scholarship. Computational resources were provided by the Australian National Computational Infrastructure through the National Computational Merit Allocation Scheme, and by the University of Queensland Research Computing Centre. Open Access publishing facilitated by The University of Adelaide, as part of the Wiley - The University of Adelaide agreement via the Council of Australian University Librarians.

Conflict of Interests

The authors declare no conflict of interest.

Data Availability Statement

The data that support the findings of this study are available in the supplementary material of this article.

Keywords: cytochrome P450 enzymes · enzyme mechanism · heterocycles · metalloenzymes · X-ray crystallography

[1] P. Bhutani, G. Joshi, N. Raja, N. Bachhav, P. K. Rajanna, H. Bhutani, A. T. Paul, R. Kumar, *J. Med. Chem.* **2021**, *64*, 2339–2381.
[2] a) B. R. Smith, C. M. Eastman, J. T. Njardarson, *J. Med. Chem.* **2014**, *57*, 9764–9773; b) E. A. Ilardi, E. Vitaku, J. T. Njardarson, *J. Med. Chem.* **2014**, *57*, 2832–2842.
[3] R. D. Taylor, M. MacCoss, A. D. Lawson, *J. Med. Chem.* **2014**, *57*, 5845–5859.
[4] L. A. Peterson, *Chem. Res. Toxicol.* **2013**, *26*, 6–25.
[5] G. E. Davico, V. M. Bierbaum, C. H. DePuy, G. B. Ellison, R. R. Squires, *J. Am. Chem. Soc.* **1995**, *117*, 2590–2599.
[6] a) J. T. Groves, G. A. McClusky, *J. Am. Chem. Soc.* **1976**, *98*, 859–861; b) C. M. Krest, A. Silakov, J. Rittle, T. H. Yosca, E. L. Onderko, J. C. Calixto, M. T. Green, *Nat. Chem.* **2015**, *7*, 696–702; c) J. Rittle, M. T. Green, *Science* **2010**, *330*, 933–937.
[7] a) M. Asaka, H. Fujii, *J. Am. Chem. Soc.* **2016**, *138*, 8048–8051; b) C. M. Bathelt, L. Ridder, A. J. Mulholland, J. N. Harvey, *Org. Biomol. Chem.* **2004**, *2*, 2998–3005; c) T. Coleman, A. M. Kirk, J. H. Z. Lee, D. Z. Doherty, J. B. Bruning, E. H. Krenske, J. J. De Voss, S. G. Bell, *ACS Catal.* **2022**, *12*, 1258–1267.
[8] a) G. Guroff, J. W. Daly, D. M. Jerina, J. Renson, B. Witkop, S. Udenfriend, *Science* **1967**, *157*, 1524–1530; b) J. Koerts, A. E. Soffers, J. Vervoort, A. De Jager, I. M. Rietjens, *Chem. Res. Toxicol.* **1998**, *11*, 503–512.
[9] a) H. G. Selander, D. M. Jerina, J. W. Daly, *Arch. Biochem. Biophys.* **1975**, *168*, 309–321; b) H. G. Selander, D. M. Jerina, D. E. Piccolo, G. A. Berchtold, *J. Am. Chem. Soc.* **1975**, *97*, 4428–4430; c) M. R. Lovern, M. J. Turner, M. Meyer, G. L. Kedderis, W. E. Bechtold, P. M. Schlosser, *Carcinogenesis* **1997**, *18*, 1695–1700; d) A. B. Lindstrom, K. Yeowell-O'Connell, S. Waidyanatha, B. T. Golding, R. Tornero-Velez, S. M. Rappaport, *Carcinogenesis* **1997**, *18*, 1637–1641; e) J. E. Stok, S. Chow, E. H. Krenske, C. Farfan Soto, C. Matyas, R. A. Poirier, C. M. Williams, J. J. De Voss, *Chemistry* **2016**, *22*, 4408–4412.
[10] a) S. Shaik, S. Cohen, Y. Wang, H. Chen, D. Kumar, W. Thiel, *Chem. Rev.* **2010**, *110*, 949–1017; b) S. Shaik, P. Milko, P. Schyman, D. Usharani, H. Chen, *J. Chem. Theory Comput.* **2011**, *7*, 327–339; c) C. M. Bathelt, A. J. Mulholland, J. N. Harvey, *J. Phys. Chem. A* **2008**, *112*, 13149–13156; d) R. P. Hanzlik, K. Hogberg, C. M. Judson, *Biochemistry* **1984**, *23*, 3048–3055.
[11] B. Meunier, S. P. de Visser, S. Shaik, *Chem. Rev.* **2004**, *104*, 3947–3980.
[12] a) M. D. Delost, D. T. Smith, B. J. Anderson, J. T. Njardarson, *J. Med. Chem.* **2018**, *61*, 10996–11020; b) S. Pathania, R. K. Narang, R. K. Rawal, *Eur. J. Med. Chem.* **2019**, *180*, 486–508.
[13] M. A. Correia, P. F. Hollenberg, *Inhibition of Cytochrome P450 Enzymes*, (Ed. P. R. Ortiz de Montellano), Springer International Publishing, Cham, **2015**, pp. 177–259.
[14] a) M. N. Podgorski, T. Coleman, P. D. Giang, C. R. Wang, J. B. Bruning, P. V. Bernhardt, J. J. De Voss, S. G. Bell, *Inorg. Chem.* **2022**, *61*, 236–245; b) M. N. Podgorski, T. Coleman, R. R. Chao, J. J. De Voss, J. B. Bruning, S. G. Bell, *J. Inorg. Biochem.* **2020**, *203*, 110913.
[15] a) L. L. Koenigs, W. F. Trager, *Biochemistry* **1998**, *37*, 13184–13193; b) L. L. Koenigs, W. F. Trager, *Biochemistry* **1998**, *37*, 10047–10061; c) H. Li, Y. Peng, J. Zheng in *Chapter Two - Metabolic Activation and Toxicities of Furanoterpenoids, Vol. 10* Eds.: J. C. Fishbein, J. M. Heilman), Elsevier, **2016**, pp. 55–97.
[16] S. C. Khojasteh-Bakht, W. Chen, L. L. Koenigs, R. M. Peter, S. D. Nelson, *Drug Metab. Dispos.* **1999**, *27*, 574–580.
[17] a) L. A. Gates, D. Lu, L. A. Peterson, *Drug Metab. Dispos.* **2012**, *40*, 596–601; b) D. Lu, L. A. Peterson, *Chem. Res. Toxicol.* **2010**, *23*, 142–151; c) L. A. Peterson, *Drug Metab. Rev.* **2006**, *38*, 615–626; d) L. A. Peterson, M. E. Cummings, C. C. Vu, B. A. Matter, *Drug Metab. Dispos.* **2005**, *33*, 1453–1458.
[18] a) P. M. Dansette, G. Bertho, D. Mansuy, *Biochem. Biophys. Res. Commun.* **2005**, *338*, 450–455; b) D. Mansuy, P. M. Dansette, *Adv. Exp. Med. Biol.* **1996**, *387*, 1–6; c) D. Mansuy, P. M. Dansette, C. Foures, M. Jaouen, G. Moinet, N. Bayer, *Biochem. Pharmacol.* **1984**, *33*, 1429–1435; d) E. Neau, P. M. Dansette, V. Andronik, D. Mansuy, *Biochem. Pharmacol.* **1990**, *39*, 1101–1107; e) P. M. Rademacher, C. M. Woods, Q. Huang, G. D. Szklarz, S. D. Nelson, *Chem. Res. Toxicol.* **2012**, *25*, 895–903.
[19] M. P. López-Garcia, P. M. Dansette, D. Mansuy, *Biochemistry* **1994**, *33*, 166–175.
[20] A. Treiber, P. M. Dansette, H. El Amri, J.-P. Girault, D. Ginderow, J.-P. Mornon, D. Mansuy, *J. Am. Chem. Soc.* **1997**, *119*, 1565–1571.
[21] a) T. Coleman, R. R. Chao, J. B. Bruning, J. De Voss, S. G. Bell, *RSC Adv.* **2015**, *5*, 52007–52018; b) T. Coleman, S. H. Wong, M. N. Podgorski, J. B. Bruning, J. J. De Voss, S. G. Bell, *ACS Catal.* **2018**, *8*, 5915–5927; c) T. Coleman, J. E. Stok, M. N. Podgorski, J. B. Bruning, J. J. De Voss, S. G. Bell, *J. Biol. Inorg. Chem.* **2020**; d) T. Coleman, A. M. Kirk, R. R. Chao, M. N. Podgorski, J. S. Harbort, L. R. Churchman, J. B. Bruning, P. V. Bernhardt, J. R. Harmer, E. H. Krenske, J. J. De Voss, S. G. Bell, *ACS Catal.* **2021**, *11*, 1995–2010.
[22] a) S. G. Bell, A. B. Tan, E. O. Johnson, L. L. Wong, *Mol. BioSyst.* **2010**, *6*, 206–214; b) S. G. Bell, W. Yang, A. B. Tan, R. Zhou, E. O. Johnson, A. Zhang, W. Zhou, Z. Rao, L. L. Wong, *Dalton Trans.* **2012**, *41*, 8703–8714; c) S. G. Bell, R. Zhou, W. Yang, A. B. Tan, A. S. Gentleman, L. L. Wong, W. Zhou, *Chemistry* **2012**, *18*, 16677–16688; d) M. N. Podgorski, T. Coleman, L. R. Churchman, J. B. Bruning, J. J. De Voss, S. G. Bell, *Chemistry* **2022**, *28*, e202202428; e) J. C. Miller, J. H. Z. Lee, M. A. McLean, R. R. Chao,

I. S. J. Stone, T. L. Pukala, J. B. Bruning, J. J. De Voss, M. A. Schuler, S. G. Sligar, S. G. Bell, *J. Am. Chem. Soc.* **2023**, *145*, 9207–9222.
[23] M. N. Podgorski, J. S. Harbort, T. Coleman, J. E. Stok, J. A. Yorke, L. L. Wong, J. B. Bruning, P. V. Bernhardt, J. J. De Voss, J. R. Harmer, S. G. Bell, *Biochemistry* **2020**, *59*, 1038–1050.
[24] a) J. C. Erve, W. Demaio, R. E. Talaat, *Rapid Commun. Mass Spectrom.* **2008**, *22*, 3015–3026; b) J. C. Erve, S. C. Vashishtha, W. DeMaio, R. E. Talaat, *Drug Metab. Dispos.* **2007**, *35*, 908–916; c) J. C. Erve, S. C. Vashishtha, O. Ojewoye, A. Adedoyin, R. Espina, W. Demaio, R. E. Talaat, *Xenobiotica* **2008**, *38*, 540–558.
[25] a) S. Kamel, S. Harriman, *Drug Discovery Today Technol.* **2013**, *10*, e177–e189; b) M. C. Byrns, C. C. Vu, J. W. Neidigh, J. L. Abad, R. A. Jones, L. A. Peterson, *Chem. Res. Toxicol.* **2006**, *19*, 414–420.
[26] S. Dezvarei, J. H. Z. Lee, S. G. Bell, *Enzyme Microb. Technol.* **2018**, *111*, 29–37.
[27] I. Amunom, L. J. Dieter, V. Tamasi, J. Cai, D. J. Conklin, S. Srivastava, M. V. Martin, F. P. Guengerich, R. A. Prough, *Chem. Res. Toxicol.* **2011**, *24*, 1223–1230.
[28] D. Lu, M. M. Sullivan, M. B. Phillips, L. A. Peterson, *Chem. Res. Toxicol.* **2009**, *22*, 997–1007.
[29] a) D. R. Boyd, N. D. Sharma, N. Gunaratne, S. A. Haughey, M. A. Kennedy, J. F. Malone, C. C. Allen, H. Dalton, *Org. Biomol. Chem.* **2003**, *1*, 984–994; b) D. R. Boyd, N. D. Sharma, P. J. Stevenson, P. Hoering, C. C. R. Allen, P. M. Dansette, *Int. J. Mol. Sci.* **2022**, *23*.
[30] Y. Lu, Z. Dong, P. Wang, H.-B. Zhou in *Thiophene Oxidation and Reduction Chemistry*, (Ed. J. A. Joule), Springer International Publishing, Cham, **2015**, pp. 227–293.
[31] a) N. D. Heindel, R. A. Conley, J. A. Minatelli, D. H. Boschelli, *J. Org. Chem.* **1983**, *48*, 3051–3053; b) A. I. Kosak, R. J. F. Palchak, W. A. Steele, C. M. Selwitz, *J. Am. Chem. Soc.* **1954**, *76*, 4450–4454.
[32] P. M. Dansette, S. Thébault, L. Durand-Gasselin, D. Mansuy, *9th International International society for the study of xenobiotics Meeting* (Istambul, Turkey) **2010**.
[33] a) Y. Zhao, D. G. Truhlar, *Theor. Chem. Acc.* **2007**, *120*, 215–241; b) F. Weigend, R. Ahlrichs, *Phys. Chem. Chem. Phys.* **2005**, *7*, 3297–3305; c) A. V. Marenich, C. J. Cramer, D. G. Truhlar, *J. Phys. Chem. B* **2009**, *113*, 6378–6396; d) A. D. Becke, *J. Chem. Phys.* **1993**, *98*, 5648–5652; e) S. Grimme, S. Ehrlich, L. Goerigk, *J. Comput. Chem.* **2011**, *32*, 1456–1465; f) W. J. Hehre, R. Ditchfield, J. A. Pople, *J. Chem. Phys.* **1972**, *56*, 2257–2261.
[34] a) T. Otani, J. Takayama, Y. Sugihara, A. Ishii, J. Nakayama, *J. Am. Chem. Soc.* **2003**, *125*, 8255–8263; b) J. Takayama, Y. Sugihara, T. Takayanagi, J. Nakayama, *Tetrahedron Lett.* **2005**, *46*, 4165–4169.
[35] B. J. Levandowski, D. Herath, N. M. Gallup, K. N. Houk, *J. Org. Chem.* **2018**, *83*, 2611–2616.
[36] L. Toma, S. Romano, P. Quadrelli, P. Caramella, *Tetrahedron Lett.* **2001**, *42*, 5077–5080.
[37] B. Wang, C. Li, K. B. Cho, W. Nam, S. Shaik, *J. Chem. Theory Comput.* **2013**, *9*, 2519–2525.
[38] J. Morrison, *Biochim. Biophys. Acta Enzymol.* **1969**, *185*, 269–286.
[39] A. Glieder, P. Meinhold in *High-Throughput Screens Based on NAD(P)H Depletion*, Eds.: F. H. Arnold, G. Georgiou), Humana Press, Totowa, NJ, **2003**, pp. 157–170.
[40] a) M. E. Albertolle, F. Peter Guengerich, *J. Inorg. Biochem.* **2018**, *186*, 228–234; b) C. J. C. Whitehouse, S. G. Bell, L.-L. Wong, *Chem. Soc. Rev.* **2012**, *41*, 1218–1260.
[41] M. J. Frisch, G. W. Trucks, H. B. Schlegel, G. E. Scuseria, M. A. Robb, J. R. Cheeseman, G. Scalmani, V. Barone, G. A. Petersson, H. Nakatsuji, X. Li, M. Caricato, A. V. Marenich, J. Bloino, B. G. Janesko, R. Gomperts, B. Mennucci, H. P. Hratchian, J. V. Ortiz, A. F. Izmaylov, J. L. Sonnenberg, Williams, F. Ding, F. Lipparini, F. Egidi, J. Goings, B. Peng, A. Petrone, T. Henderson, D. Ranasinghe, V. G. Zakrzewski, J. Gao, N. Rega, G. Zheng, W. Liang, M. Hada, M. Ehara, K. Toyota, R. Fukuda, J. Hasegawa, M. Ishida, T. Nakajima, Y. Honda, O. Kitao, H. Nakai, T. Vreven, K. Throssell, J. A. Montgomery Jr., J. E. Peralta, F. Ogliaro, M. J. Bearpark, J. J. Heyd, E. N. Brothers, K. N. Kudin, V. N. Staroverov, T. A. Keith, R. Kobayashi, J. Normand, K. Raghavachari, A. P. Rendell, J. C. Burant, S. S. Iyengar, J. Tomasi, M. Cossi, J. M. Millam, M. Klene, C. Adamo, R. Cammi, J. W. Ochterski, R. L. Martin, K. Morokuma, O. Farkas, J. B. Foresman, D. J. Fox in *Gaussian 16 Rev. C.01*, *Vol.* Wallingford, CT, **2016**.
[42] M. S. Teynor, N. Wohlgemuth, L. Carlson, J. Huang, S. L. Pugh, B. O. Grant, R. S. Hamilton, R. Carlsen, E. D. H. in *Milo*, Revision 1.0.3, Brigham Young University, Provo UT, **2021**, https://github.com/DanielEss-lab/milo.
[43] D. Aragão, J. Aishima, H. Cherukuvada, R. Clarken, M. Clift, N. P. Cowieson, D. J. Ericsson, C. L. Gee, S. Macedo, N. Mudie, S. Panjikar, J. R. Price, A. Riboldi-Tunnicliffe, R. Rostan, R. Williamson, T. T. Caradoc-Davies, *J. Synchrotron Radiat.* **2018**, *25*, 885–891.
[44] P. Legrand, XDSME: XDS Made Easier (2017) GitHub repository, https://github.com/legrandp/xdsme, DOI 10.5281/zenodo.837885.
[45] P. R. Evans, G. N. Murshudov, *Acta Crystallogr. Sect. D* **2013**, *69*, 1204–1214.
[46] T. G. G. Battye, L. Kontogiannis, O. Johnson, H. R. Powell, A. G. W. Leslie, *Acta Crystallogr. Sect. D* **2011**, *67*, 271–281.
[47] A. J. McCoy, R. W. Grosse-Kunstleve, P. D. Adams, M. D. Winn, L. C. Storoni, R. J. Read, *J. Appl. Crystallogr.* **2007**, *40*, 658–674.
[48] P. Emsley, B. Lohkamp, W. G. Scott, K. Cowtan, *Acta Crystallogr. Sect. D* **2010**, *66*, 486–501.
[49] N. W. Moriarty, R. W. Grosse-Kunstleve, P. D. Adams, *Acta Crystallogr. Sect. D* **2009**, *65*, 1074–1080.
[50] P. V. Afonine, R. W. Grosse-Kunstleve, N. Echols, J. J. Headd, N. W. Moriarty, M. Mustyakimov, T. C. Terwilliger, A. Urzhumtsev, P. H. Zwart, P. D. Adams, *Acta Crystallogr. Sect. D* **2012**, *68*, 352–367.
[51] V. B. Chen, W. B. Arendall III, J. J. Headd, D. A. Keedy, R. M. Immormino, G. J. Kapral, L. W. Murray, J. S. Richardson, D. C. Richardson, *Acta Crystallogr. Sect. D* **2010**, *66*, 12–21.
[52] P. V. Afonine, N. W. Moriarty, M. Mustyakimov, O. V. Sobolev, T. C. Terwilliger, D. Turk, A. Urzhumtsev, P. D. Adams, *Acta Crystallogr. Sect. D* **2015**, *71*, 646–666.
[53] T. C. Terwilliger, R. W. Grosse-Kunstleve, P. V. Afonine, N. W. Moriarty, P. D. Adams, R. J. Read, P. H. Zwart, L.-W. Hung, *Acta Crystallogr. Sect. D* **2008**, *64*, 515–524.
[54] D. Liebschner, P. V. Afonine, N. W. Moriarty, B. K. Poon, O. V. Sobolev, T. C. Terwilliger, P. D. Adams, *Acta Crystallogr. Sect. D* **2017**, *73*, 148–157.
[55] Schrodinger, LLC in *The PyMOL Molecular Graphics System, Version 1.4.1*, *Vol.* **2015**.
[56] E. F. Pettersen, T. D. Goddard, C. C. Huang, G. S. Couch, D. M. Greenblatt, E. C. Meng, T. E. Ferrin, *J. Comput. Chem.* **2004**, *25*, 1605–1612.
[57] R. Lonsdale, J. Oláh, A. J. Mulholland, J. N. Harvey, *J. Am. Chem. Soc.* **2011**, *133*, 15464–15474.
[58] M. Yoshida, Y. Katagiri, W. B. Zhu, K. Shishido, *Org. Biomol. Chem.* **2009**, *7*, 4062–4066.
[59] M. Karplus, *J. Am. Chem. Soc.* **1963**, *85*, 2870–2871.
[60] a) Y. Li, T. Thiemann, T. Sawada, S. Mataka, M. Tashiro, *J. Org. Chem.* **1997**, *62*, 7926–7936; b) T. Thiemann, J. Iniesta, D. J. Walton, *Phosphorus Sulfur Silicon Relat. Elem.* **2016**, *191*, 876–884.
[61] N. H. Werstiuk, J. Ma, *Can. J. Chem.* **1994**, *72*, 2493–2505.
[62] C. S. Wannere, A. Paul, R. Herges, K. N. Houk, H. F. Schaefer, 3rd, P. von Ragué Schleyer, *J. Comput. Chem.* **2007**, *28*, 344–361.
[63] R. A. Boto, F. Peccati, R. Laplaza, C. Quan, A. Carbone, J. P. Piquemal, Y. Maday, A. J. Contreras-Garci, *J. Chem. Theory Comput.* **2020**, *16*, 4150–4158.
[64] D. H. Ess, K. N. Houk, *J. Am. Chem. Soc.* **2007**, *129*, 10646–10647.

Manuscript received: April 30, 2023
Accepted manuscript online: June 20, 2023
Version of record online: August 2, 2023